UNIVERSITY OF SOUTHAMPTON

DISSERTATION

High-fidelity Ground Risk Mapping and Pathfinding for Drone Flight Corridors

Author
Jiun TAY

Supervisor
Professor Tom CHERRETT
Co-supervisor: Aliaksei Pilko

This report is submitted in partial fulfilment of the requirements for the MEng Aeronautics and Astronautics, Faculty of Engineering and the Environment, University of Southampton.

Word Count: 10,755

3rd May 2022

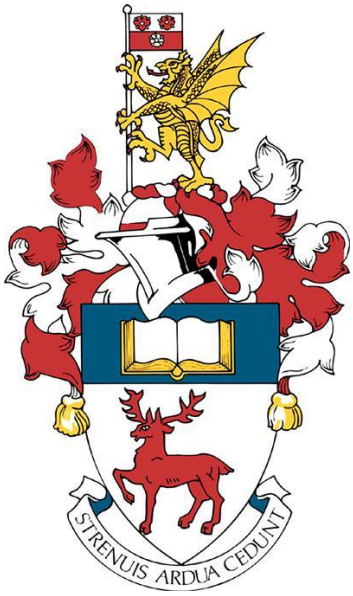

Declaration of Authorship

I, Jiun Tay, declare that this thesis and the work presented in it are my own and has been generated by me as the result of my own original research. I confirm that:

- This work was done wholly or mainly while in candidature for a degree at this University;
- Where any part of this thesis has previously been submitted for any other qualification at this University or any other institution, this has been clearly stated;
- Where I have consulted the published work of others, this is always clearly attributed;
- Where I have quoted from the work of others, the source is always given. With the exception of such quotations, this thesis is entirely my own work;
- I have acknowledged all main sources of help;
- Where the thesis is based on work done by myself jointly with others, I have made clear exactly what was done by others and what I have contributed myself;
- None of this work has been published before submission.

Acknowledgements

I would like to thank my supervisor Professor Tom Cherrett for the opportunity to work on this project and for his insights on the individual project, Aliaksei Pilko and Zachary Tait for their support on programming an extension to the SEEDPOD Ground Risk Model application used in this work, as well as Professor David Martin for his guidance in assembling the data sources.

Abstract

The use of Uncrewed Aerial Systems (UASs or drones) has been exponentially increasing over recent years and is forecast to continue into the mid-2020s. With a rising number of UASs flying Beyond Visual Line of Sight (BVLoS), greater emphasis must be placed on developing suitable ground models for automated flightpath routing and risk mitigation. This paper makes use of census data from 2011 to simulate spatiotemporal population distributions within Southampton to understand how ground risks can be best mitigated in UAS route design. These distributions are then compared with previous works based on the National Human Activity Pattern Survey conducted in the USA around the early 90's. Further analysis between the two datasets explores population changes over the first decade of the 21st century and the application of the methodology to the wider Hampshire county assesses its validity. Ultimately, recommendations were made on the safety of automated drone route planning via a risk-distance compromise and the feasibility of drone logistics systems when considering the changing number of people below flight corridors is determined. It was found that risk did not significantly change when routing via sparsely populated areas, but it can be reduced over high-trafficked regions by choosing specific delivery times throughout the day.

Contents

Acronyms

AAIB	Air Accidents Investigation Branch
AI	Artificial Intelligence
BVLoS	Beyond Visual Line of Sight
C2	Command and Control
CAA	Civil Aviation Authority
CPD	Crash Probability Density
DAA	Detect and Avoid
EASA	European Union Aviation Safety Agency
EU	European Union
GIS	Geographic Information System
FRZ	Flight Restricted Zone
KE	Kinetic Energy
LoC	Loss of Control
MTOW	Maximum Take-off Weight
NHAPS	National Human Activity Pattern Survey
NHS	National Health Service
NOTAMs	Notices to Airmen
OSM	Open Street Map
PNR	Non-Residential Population
PR	Residential Population
PT	Population in Transit
QA	Quality Assurance
SORA	Specified Operations Risk Assessment
TIFF	Tagged Image File Format
UASs	Uncrewed Aerial Systems
UK	United Kingdom
UTM	Uncrewed Traffic Management
VLL	Very Low Level
VLoS	Visual Line of Sight
VTOL	Vertical Take-Off and Landing
WVLoS	Within Visual Line of Sight

1 Introduction

The number of Uncrewed Aerial Systems (UASs) operating in the skies annually has been exponentially increasing and is forecast to continue doing so into the mid-2020s as seen in Figure 1. This is mainly prevalent in the commercial sector with developments in recent years introducing UASs for surveying and medical logistics alongside existing ventures such as Amazon Prime Air and UPS Flight Forward (Ueland, 2021) spearheading drone delivery progress. Although the feasibility of such operations is an emotive topic with the recent reduction of Prime Air's UK team (Kersley, 2021) casting doubts on the future of a global drone delivery network due to the engineering challenges that heavier drones require extra regulations to protect people on the ground from potential collisions, this paper focusses solely on the risk mapping aspects of UASs mission planning and execution.

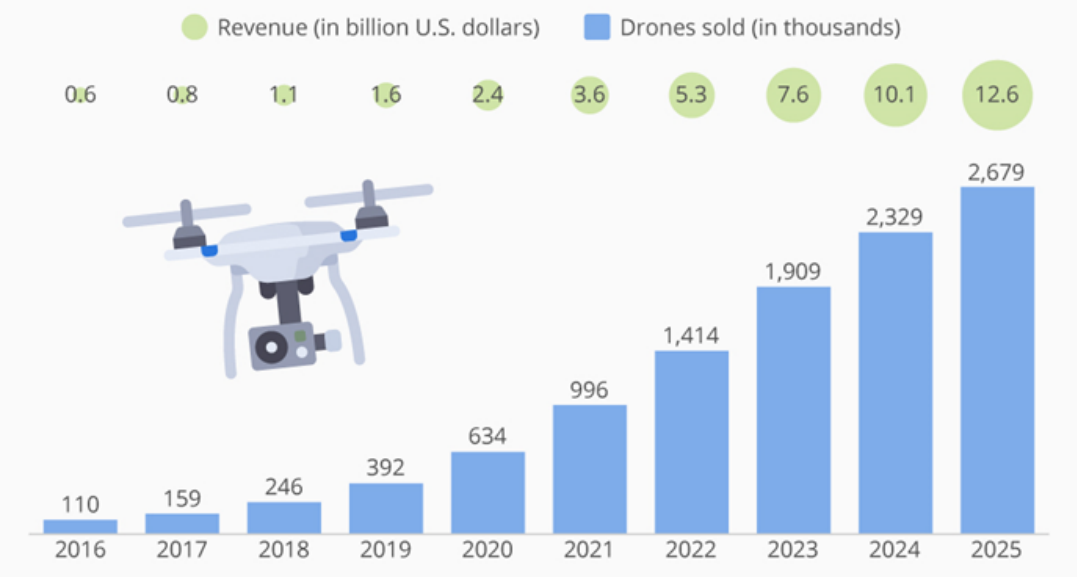

Figure 1: Projected worldwide market growth for commercial drones (Buchholz, 2019).

With an increasing number of UASs in operation, it is infeasible to assume that every single UAS would be flown by a single pilot with Visual Line of Sight (VLoS) via Command and Control (C2) Link. After all, with automation, a single operator could instead theoretically oversee tens to hundreds of drones, reducing the expenditure needed as compared to the current labour-intensive structure. Furthermore, UASs are capable of remote and rapid delivery as they are detached from the road system that conventional logistics services use. This allows for innovative distribution of goods such as timely delivery of medical items to rural locations (Ghelichi et al., 2021) which would otherwise take too long through regular mail. However, the infancy of drone risk assessment legislations means that there is a significant level of risk that has yet to be addressed. Current laws require UAS pilots flying BVLoS to submit an operating safety case before operating but apart from knowledge of the aircraft and assumptions made from weather and ground reports, there is no substantial and accurate method to determine risk.

2 Aims & Objectives

The goal of this project is to improve upon the generation of existing spatiotemporal risk maps by Pilko et al. (2022) with a higher fidelity population model. The work of Martin et al. (2015) and open software Population24/7, utilising 2011 census data from the Office for National Statistics as well as several other sources, have been used to create more accurate mapping. In summary, the objectives are to:

- Understand the wider implications of ground risk on the ability to plan and undertake drone flights
- Integrate a higher fidelity population model to existing UAS ground risk map generation software
- Test the model using a week's worth of ground risk data for a 15 by 15 km region of the city of Southampton and its surrounding area with the updated software
- Quantify the changes in population between the National Human Activity Pattern Survey (NHAPS) conducted by Klepeis et al. (2001) and 2011 census data
- Evaluate the differences in the methodologies used by Pilko et al. (2022) and this paper as well as how they affect the results
- Validate the current methodology by applying it to surgeries within the wider Hampshire County that are undergoing experimental UAS trials to quantify risk

3 Literature Review

As the concept of commercial drone delivery services is still in its relative infancy, with the term entering mainstream usage around 2013 when Amazon's founder Jeff Bezos made an announcement that Amazon Prime Air was planning rapid delivery of lightweight commercial products using UASs (Pierce, 2013), there are generally two particular types of literature available for review; research papers that discusses potential opportunities in which such an idea could be implemented and work focused on how this disruptive technology is perceived by the public, the ways to control it, as well as its implications. Specifically, it can be observed that current academia is split into two camps with one side embracing the theoretical future of large-scale drone delivery systems and the other taking a more grounded approach in ensuring that this idea can be properly assimilated with current legislations (Çalhan and Cicioğlu, 2022; Lemardelé et al., 2021; Kraus et al., 2020; Wright, 2014).

On the other hand, literature regarding ground risk mapping encompasses a broad range of applications, with academic papers primarily concentrated on the evolving ecosystem and the associated health risk it poses to the human population (Ajeh, 2022; Bux et al., 2022; Boloorani et al., 2021). It can also be said that this area of research has yet to be consolidated with many recent entries introducing new methods and frameworks for mapping said risks. Though the integration of UASs into Very Low Level (VLL) airspace over urban regions is likely to bring with it a whole host of issues regarding its impacts on society and the environment, they are not within the scope of this report and hence have only been briefly discussed. Instead, attention should be drawn towards one of the most essential factors in designing future drone flight corridors: the risk of human fatality.

3.1 Potential of Drone Logistic Systems

Progress in the developments of sophisticated Artificial Intelligence (AI) and economical UASs has allowed a wider range of stakeholders to invest and experiment with its application. As indicated by a recent study (Lynn, 2021) conducted with a sample size of 1,050 Singaporean residents, there is a strong public opinion favouring the usage of UASs to assist in pre-existing transport functions with the highest support of 92.10% in search and rescue operations and the lowest rated poll for transporting people at 62.00%. Drone logistic systems for delivery and pickup also have a high approval with 82.86% of participants in favour for it.

Though it is likely that the majority of respondents in this study are unaware about the difficulties of integrating UASs with highly urbanised environments, they share the same opinion with many pioneering companies in the fact that UASs may become a useful additional mode to complement current transport methods and help the sustainability of the transport network (Pugliese et al., 2020). Compared with conventional ground-based transportation, drones do not suffer from traffic jams, congested roads, or a lack of access to remote areas which makes them faster and more efficient. Computational analysis undertaken by Pugliese et al. (2020) seeks to verify this aspect and has shown that a hybrid usage of trucks paired with drones for "last mile" deliveries produced the best compromise in terms of costs, CO_2 emissions, and traffic congestion as compared to truck or drone-only systems.

This example of using UASs to improve the performance of current logistic systems is just one of the many potential applications being proposed. However, without proper legislations to assess the risk of drone operations in place and further breakthroughs in battery technology, automated drone deliveries on a major scale would be improbable (Zhang et al., 2021). Paired with the diminishing returns that longer flight times require bigger batteries and hence heavier UASs, current UASs are limited to small-scale ventures.

3.2 Current UASs Used by Industries

Although UASs have been used for years mainly by consumer hobbyists, it is only recently that they have begun to enter the market in a commercial sense. This has been typically restricted to non-disruptive tasks where failure of the UAS is unlikely to cause any further damages apart from the drone itself. As seen in Figure 2, they are most often deployed to conduct routine, dangerous, or dirty work where companies would otherwise prefer not to invest multiple employees to complete but rather a drone that is operated within Visual Line of Sight (VLoS) by a smaller team.

Their ease of use, lower barrier to entry, and relatively inexpensive way to remotely sense damages in infrastructure such as rooves and bridges for risk assessment and maintenance purposes makes them an ideal alternative to traditional inspection methods. Under the right circumstances, these automated missions could even reduce the time needed by 73% as compared to those operated by a human pilot (Rey et al., 2021). Furthermore, they are also capable of supplying a wide-area perspective of places that would otherwise be hard to reach such as swamps or mines without needing to subject a worker to potentially dangerous situations (Padró et al., 2019).

Aside from remote inspection, there are also emerging uses of UASs within the logistic industry, chiefly comprised of experiments and research projects. While scaled down and highly specific in nature, these trials serve as a basis for future establishments in the drone logistic market (Ghelichi et al., 2021).

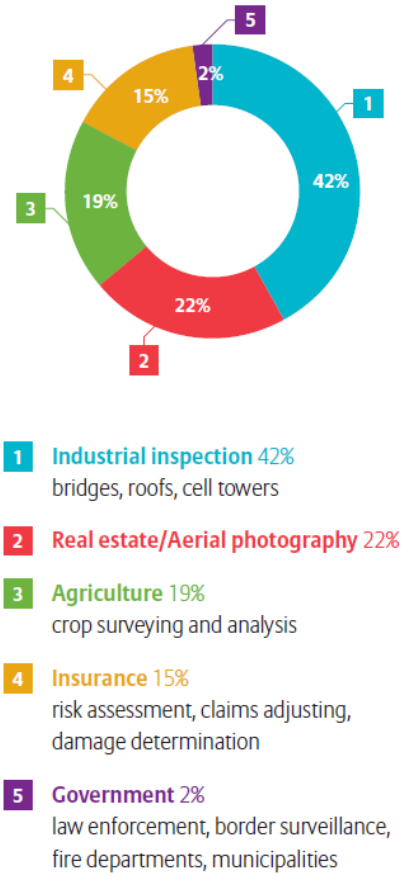

Figure 2: Top 5 UAS markets by industry (Allianz, n.d.).

3.3 Future Market Predictions

If the challenges and operating restrictions of integrating UASs into current airspace systems could be overcome by future regulations as outlined by Dalamagkidis et al. (2008), some predictions could be made about the different types of logistic operations employed. These can be subdivided into three distinct categories (Embention, 2021):

- General Cargo Logistics

  This includes the long-range distribution of all kinds of goods. For example, cargo activities over highly populated areas, in remote areas such as islands, as well as allocation between logistic centres. While possible in assisting current road-based transportation of cargo, potential issues include:

  - Freight-like containers require large UASs capable of carrying heavy loads
  - Risk assessment would be mandatory for passage over urban territories
  - Until substantial testing and safety certifications have been achieved, operations would likely still be within non-populated areas only

- Express Cargo Logistics

  For this kind of services, both the flight time and payload would be significantly shorter/lighter as compared to the bulk shipping of goods. Apart from rapid point-to-point delivery of small objects like food or parcels, UASs under this category can be paired with existing forms of transportation such as the truck-drone model (Pugliese et al., 2020) to reduce costs and improve efficiency. Due to the relatively low barrier to entry smaller UASs benefit from, this market is shaping up to become one of the most heavily invested areas of drone logistic research. Though this category roughly encapsulates most peoples' idea of a future with drone deliveries, notable points are that:

  - High number of UASs in operation would require an Uncrewed Traffic Management (UTM) system such as that proposed by Jiang et al. (2016) to ensure that autonomous flightpaths do not collide with one another
  - Security, safety, and privacy concerns for home deliveries. More work has to be done into determining the best way for UASs to land in a specified area of a compound and to ensure customers are not harmed by UAS motion during collection.
  - Depending on delivery frequencies, UAS capabilities, and logistics management of the service provider, express drone deliveries may either be a single point-to-point transaction or could potentially mimic traditional "milk-round" van routes where multiple collections/deliveries could be efficiently done in a single flight.

- Surveillance

  Lastly, the future usage of UASs would not only be limited to carrying a payload around. As seen in the previous section, the majority of current drone utilisation is actually focused on remote sensing operations. Acting essentially as a controllable flying camera, UASs would be able to cover the surveillance of a logistic network over a large area. This category is already in development with Network Rail (2021) recently completing a proof-of-concept 25-kilometre BVLoS UAS flight along the East West Rail as a test for how drones can be used to inspect railways quickly, safely, and cost-effectively. Before operations like this can be more commonplace, a few points to consider includes:

  - If UASs are constantly patrolling the same route, potential for high noise pollution unless quieter blades and motors are developed and implemented
  - Cost analysis between competing methods should be conducted for different applications. Conventionally fixed cameras might be able to yield the same results with a lower expense

These three categories are sufficient in covering the vast range of potential utilisation of drone logistic systems in the future. With this knowledge, steps can now be taken to ease the introduction of UASs into our airspace. In order to understand the risks this future market would bring, we would need to first establish the current laws in place and how its shortcomings may lead to certain implications when a drone inevitably crashes.

3.4 UK Drone Laws and Regulations

Current assessment of the drone industry shows that there is a significant gap in the laws and regulations regarding UAS operations (Dalamagkidis et al., 2008). Unlike the decades of experience civil aviation has, the rise and evolution of UASs have been too rapid for legislators to keep up. As UASs are drastically smaller and less complex than wide-body aircrafts, what took multinational corporations several years and billions of dollars to develop could now be done by any inspiring start-up with just a fraction of the investment. This ease of entering the market has meant that the advancement in drone technology would continue at breakneck speeds.

Furthermore, as prices continue to drop, the number of drone hobbyist grows as well. Consumers who build their own UASs or purchase them online do not have the same level of Quality Assurance (QA) one would expect from aircraft manufacturers. Cheap drones with poor QA that are flown by inexperienced pilots are one of the major risks that is poorly regulated. Though exact statistics of this is difficult to obtain due to the relative infancy of the subject, some experts estimate that one-third of all UAS owners will at some point experience a crash with a recently conducted survey (Ciobanu, 2021) showing the startling percentage that 56.5% of respondents have crashed their drones at least 1 to 5 times with a further 9.7% of them reporting a crash frequency of 5 or more times.

Despite the efforts of regulatory bodies, it is evident that current legislation and standards are not fit in guaranteeing the safety of UASs operations. One notable example includes the 2019 incident in which a remotely piloted Alauda Airspeeder Mk II crashed within the Goodwood Aerodrome while giving a flight demonstration (Calderwood, 2021). The pilot lost control mid-flight and an emergency kill switch failed to activate due to a damaged relay resulting in the UAS climbing to approximately 8,000 feet into controlled airspace around Gatwick Airport. Once its batteries were depleted, the drone crashed into a field of crops barely 40 metres from occupied houses and was 700 metres outside its designated operating area. Thankfully, there were no injuries. Subsequent investigations by the Air Accidents Investigation Branch (AAIB) revealed a number of issues with the design and build of the UAS, including numerous single point failures. The report (AAIB, 2021) also exposed the failures of the Civil Aviation Authority (CAA) in approving the UAS which ultimately led to the AAIB issuing no fewer than 15 safety recommendations as well as the CAA introducing new measures to address these issues.

As of January 1st, 2021, the United Kingdom (UK) withdrew from the European Union Aviation Safety Agency (EASA) system (CAA, 2021). However, as these legislations are merely frozen in time and are still applicable, the remainder of this paragraph will provide a brief recap of the EASA's drone regulations. EASA categorises UASs operations into three broad categories in order of ascending perceived risk levels. From Article 4, 5, and 6 in EUR-Lex (2019), these are the "Open" category which is further broken down to multiple subcategories based largely on aircraft abilities and geo-awareness where pilots may be inexperienced and some operations can be conducted without submitting any documents; the "Specific" category where UASs operation(s) do not meet the previous class – usually due to the aircraft's Maximum Take-off Weight (MTOW) being too high – and a case-by-case authorisation based on risk assessments is required for all missions; as well as the "Certified" category in which the UAS is analogous to light manned aircrafts and share much of the same base regulations. This class requires all UASs and their operators to have proper certification plus licensing and is the only category which could allow the overflight of large assemblies of people or the transportation of dangerous goods.

Moving on from the EASA system to that of the CAA, there are many statutes that are relevant for UASs operations occurring over property in VLL airspace. These includes (without amendments) the Civil Aviation Act (1982) and The Air Navigation Order, (2016). There are

no mentions of airspace ownership in these legislations as it is widely understood that airspace is a state asset. However, it can be noted that the airspace is divided into 3-dimensional blocks which falls under a few controlled classes A, C, D, E, as well as the uncontrolled class G (CAA, 2021). Most drone hobbyists flying relatively light and inexpensive commercial UASs in class G airspace far away from other people would fall under the Open A3 category which has similar basic requirements to the old UK rules that were previously in place. Flying closer to people past specific distance thresholds would fall under the higher subcategories A2 and A1, which have an increasing number of restrictions.

Generally, for these open categories, pilots are not allowed to fly over restricted airspace and have to avoid planning flightpaths along hazards such as events and emergency incidents reported by Notices to Airmen (NOTAMs). There is a legal height limit of 120 metres from the closest point on the Earth's surface to reduce the risk of coming across other aircrafts. While in operation, constant VLoS must be established between the pilot and UAS. The closest a drone can come within groups of people should also adhere to the 1:1 rule where the UAS is at least as far laterally from them as it is high from the ground.

On the other hand, and perhaps unsurprisingly, current CAA requirements for BVLoS operations are a lot more stringent as compared to those in the Open category as they fall into the Specific or Certified operation categories. UASs that are intended for these missions should require either a Detect and Avoid (DAA) capability in which the pilot or autonomous aircraft is able to "see and avoid" potential conflictions, a block of segregated airspace where other aircrafts apart from the UAS is not permitted to enter so that there will be no risk of collisions, or clear evidence that the operation will pose "no aviation threat" and is safe for persons and objects on the ground (CAA, 2020a). It can also be noted that the ultimate responsibility for avoiding any collision solely lies with the remote pilot in control regardless of the BVLoS flight rules the UAS is flying under. Currently, obtaining CAA permission to fly is similar to that of the EASA's Specific category with the exception that BVLoS UAS operations will not usually be approved without an acceptable DAA capability.

There is also a recommended development pathway set out by the CAA (2020b) in which the drone has to undergo three segregated flight tests in increasingly realistic environments before getting approval to operate in a non-segregated airspace but as pointed out by CAA themselves: as more solutions for ensuring proper certification of UASs are developed, commercialised, and standardised, future drone operators will be able to employ more standard approaches instead of progressing through a preliminary developmental pathway. From this statement, it is clear that current UASs regulations are just not up to par with the rate at which newer drone technologies are being developed. It is therefore essential to create a system that can determine the level of risk that UASs present to ground traffic in order to minimise the chances of fatal accidents occurring. One such method is the generation and analysis of ground risk maps.

3.5 Ground Risk Mapping

Risk maps are common tools in risk assessment. Though used in many research areas, there are few works in literature which uses them to measure the risk of UASs (Primatesta et al., 2019). A risk map is a two-dimensional map based on location which quantifies the exposure of third parties to the risk of strike/fatality caused by operating a UAS at the altitude the map is generated for. As seen in Figure 3, square cells which represent geographical areas are equidistantly spaced onto a matrix, $\mathbf{R}$ of size $N \times M$. Each cell $\mathbf{R}(i, j)$ contains an element called the risk value, which is the risk of that specific area. The discrete coordinates (i, j) are used to represent georeferenced locations (x, y) in another coordinate system. For this paper, the British National Grid (EPSG:27700) was used.

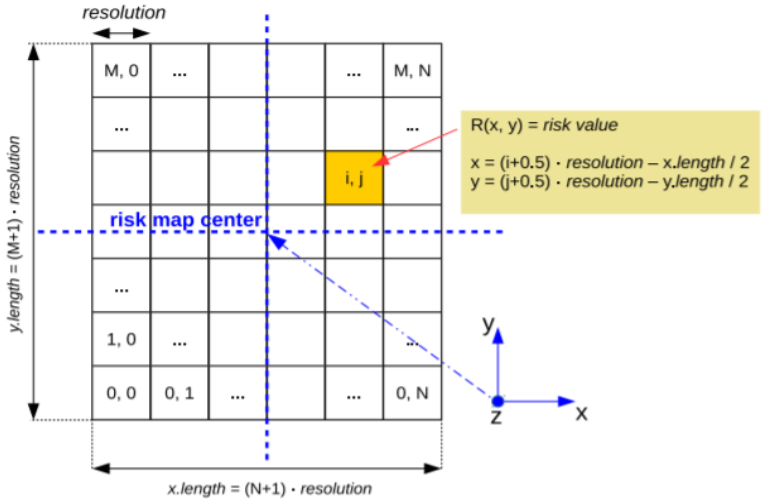

Figure 3: Representation of a risk map and its associated notations (Primatesta et al., 2019).

Risk values can be determined by a myriad of components including baseline risk levels, no-fly zones, obstacles, and presence of shelter. Conceptually, several layers each containing a specific location-based data are combined with one another to generate the map. Therefore, it is possible for significantly different results to be obtained due to the inclusion or omission of various factors. For most works (Pilko et al., 2022; Primatesta et al., 2019; Dalamagkidis et al., 2008), a probabilistic approach is taken where the chances of specific events occurring in sequence is used to calculate risk. These events are, in order of occurrence: A Loss of Control (LoC) incident in which a UAS loses control in flight, a person(s) is struck due to the uncontrolled descent, and the accident results in the person(s) being fatally injured. This model can be generally expressed with

$$P_{casualty}(x, y, t) = P_{LoC} \cdot P_{strike}(x, y, t) \cdot P_{fatality}(x, y) \tag{1}$$

where *x*, *y* are the spatial dimensions and *t* is the hour of the week. For the probability of LoC, the path a UAS takes can be simplified to either a ballistic descent in which it is a projectile with no useful lift, or it can have an uncontrolled glide. The former was used in this paper by randomly sampling the distribution of input variables to generate output distributions of the model inputs, creating a ground impact probability density function (PDF) which can then be applied to the probability of a drone at position *x*, *y* and time *t* striking a person (Pilko et al., 2022)

$$P(strike|impact)(x, y, t) = \sum PDF \cdot \rho(x, y, z) \cdot A_{exp}(\theta) \tag{2}$$

where A_{exp} is the lethal critical area and ρ is the population density. This density can be determined by the way population is modelled in the program. Finally, the major contributor in determining the risk of fatality comes from the population layer of the risk map and how well they are sheltered. This can be mathematically modelled via a logistic growth model (Dalamagkidis et al., 2008)

$$P_{fatality}(x, y) = \frac{1}{1 + \sqrt{\frac{\alpha}{\beta}} \left[\frac{\beta}{E_k^{imp}(x,y)} \right]^{\frac{1}{S(x,y)}}} \tag{3}$$

where α is the impact energy required at a shelter factor, S = 0.5 to produce a 50% probability of fatality, β is the minimum impact energy which results in fatality with no shelter ($S \rightarrow 0$), and $E_k^{imp}(x, y)$ is the Kinetic Energy (KE) of the UAS during impact. As this paper was built upon previous work by Pilko et al. (2022), a shelter factor of 0.3 was assumed to ensure consistency in the calculations.

3.6 Spatiotemporal Population Models

Spatiotemporal modelling of the human population seeks to address the issue of where, when, and in what numbers are people distributed in a geographical location of interest. Just as risk maps are used in many research fields, so too is spatiotemporal information about population important for application in different areas such as spatial planning, climate change mitigation and adaptation, traffic management, migration and mobility, environmental protection, as well as risk assessment (Renner et al., 2018). As the majority of these applications demand the data to be independent from enumeration and administrative areas (Aubrecht et al., 2014), there has been a development of various methods in the past decades to decompose census data into grids with cells of regular sizes. Though the periodic counting of a population in a nation or country that is conducted by the government is the most common method used for population measurements, issues such as a lack of public participation and propriety of questions brings the accuracy of these census into question (Anderson, 2015).

As such, other novel approaches in determining population distribution are currently being investigated as well. One example is the 2014 study by Deville et al. (2014) in which mobile phone data from major carriers in Portugal and France were used to dynamically map population activity in the two countries. The dataset was anonymised by bulking more than a billion calls (text messages were excluded) made from individuals to their respective cell towers and estimating the population density of an administrative unit based on how much it intersected with the coverage area of all nearby towers approximated via a Voronoi-like tessellation (Okabe et al., 2000). With the increasing penetration of mobile phones used by the global population, large amounts of data can be readily collected everyday by phone network providers to create more accurate and dynamic population maps. It is even possible for daily changes in population distribution to be constantly updated for the benefit of studying how society responds to disease outbreaks and emergencies. However, a major inhibitor preventing this tool from becoming commonplace is the privacy concerns of sharing the location of private individuals to relevant third parties. Until changes in data protection policies are made, it is likely that more conventional and lower fidelity methods of interpolating temporal population changes from census counts would have to be used.

3.7 Similar Risk Models

3.7.1 sUAS Airworthiness Assessment Tool (sAAT)

The small UAS Airworthiness Assessment Tool (Breunig et al., 2018) was developed to help the FAA conduct its airworthiness safety risk analysis. It is a proof of concept hoping to streamline the waiver approval process of small UASs. Though similar in its method of determining risk, sAAT differs in its output. Instead of providing a risk map, it instead returns three graphs: a probability of fatality with respect to the selected impact KE, a risk meter which shows the estimated risk level against the spectrum of acceptable risk levels, and the sensitivity of parameters that drive the overall level of risk.

3.7.2 SmartSkies SORA

Unlike the sAAT model, SmartSkies SORA (Modha, 2021) doesn't focus on the path of the drone and instead relies on the pilot answering a series of "easy-to-follow" questions about the flight. It is a fully integrated Specified Operations Risk Assessment (SORA) tool to help pilots perform a risk assessment per EASA regulations. Taking in data from the weather, population, airspace classifications, strategic conflicts, and others, it seeks to match mission profiles into their classifications and hence ensure compliance to EASA and the UK standard of risk assessments.

4 Methodology

4.1 Software Design

The software is an amalgamation of previous work conducted by Pilko et al. (2022; 2021) as well as Martin et al. (2021; 2015) and is made up of the following functional sections:

1. Population Distribution Generation
    - Framework
    - Data Sources
    - Output System
2. Fatality Risk Estimation
    - GeoTIFF to risk map computation
    - Upsampling

4.1 Population Distribution Generation

The framework in which population distributions were modelled draws a distinction between the data model and the output that was derived from it. Modifiable temporal characteristics were added to spatial data via a dasymetric (Mennis, 2009; Eicher and Brewer, 2001; Wright, 1936) and volume preserving approach (Tobler, 1979) to achieve the flexibility required for spatiotemporal analysis. Essentially, temporal profiles based on human activity at different locations were used to redistribute the total population count of an area of interest across space from a fixed ancillary dataset with weights and constraints. The total population count consists of the sum of three categories defined by Martin et al. (2015) as the Residential Population (PR), Non-Residential Population (PNR), and Population in Transit (PT). These could be further divided into subgroups based on demographics such as age and economic activity. Sticking with the variables introduced in Section 1.5, the total population, P_s of a specific subgroup *s* can be found with:

$$P_{s,x,y,t} = \sum_{i}^{x,y} PR_{i,s,t} + \sum_{i}^{x,y}\sum_{j}^{K} PNR_{i,s,t} \cdot w_{i,j,t} - \sum_{i}^{x,y}\sum_{j}^{K} PNR_{j,s,t} \cdot w_{j,i,t} + \sum_{j}^{K}\sum_{k}^{K} PT_{jk,s,t} \cdot v_{jk,x,y,t} \quad (4)$$

where the spatial dimensions of a unit of analysis *x*, *y* could itself contain multiple locations *i*. Depending on the scale of the analysis, locations can be referenced either as grid cells, areas, or points. For the purpose of this case study, a grid cell situated at *x*, *y* was chosen to contain *i* points. $PR_{i,s,t}$ is the number of subgroup's *s* residential population located at *i* during a specific hour of the week, *t*. The sum of the total population present in the grid cell is increased by accounting for the non-residential population at each *i* (such as external employees entering their place of work within a grid cell), taken from all other locations *j* in the entire area of study, where $j = 1, \dots, K$, based on the specific location interaction weighting of *i* with respect to *j* at time *t*, $w_{i,j,t}$.

Similarly, the total population is decreased by the non-residential population exiting a grid cell from each *i* to go to all other locations *j*. The final term in the equation above corresponds to the population in transit through *x*, *y* at time *t* between every pair of locations *j* and *k* with a flow specific weighting $v_{jk,x,y,t}$. The locations *i* are not included in this term as every member in the population can only be counted once. As such, PT does not include the journeys that started or ended within the grid cell; these are accounted for within the PR and PNR terms. The generalised model above shares many characteristics with other

spatiotemporal modelling methods. Namely, it can be simplified by decreasing the range of *t* values used (e.g., choosing only daytime or night-time instead of specific hours), merging all subgroups to a single group, or excluding PT from the analysis.

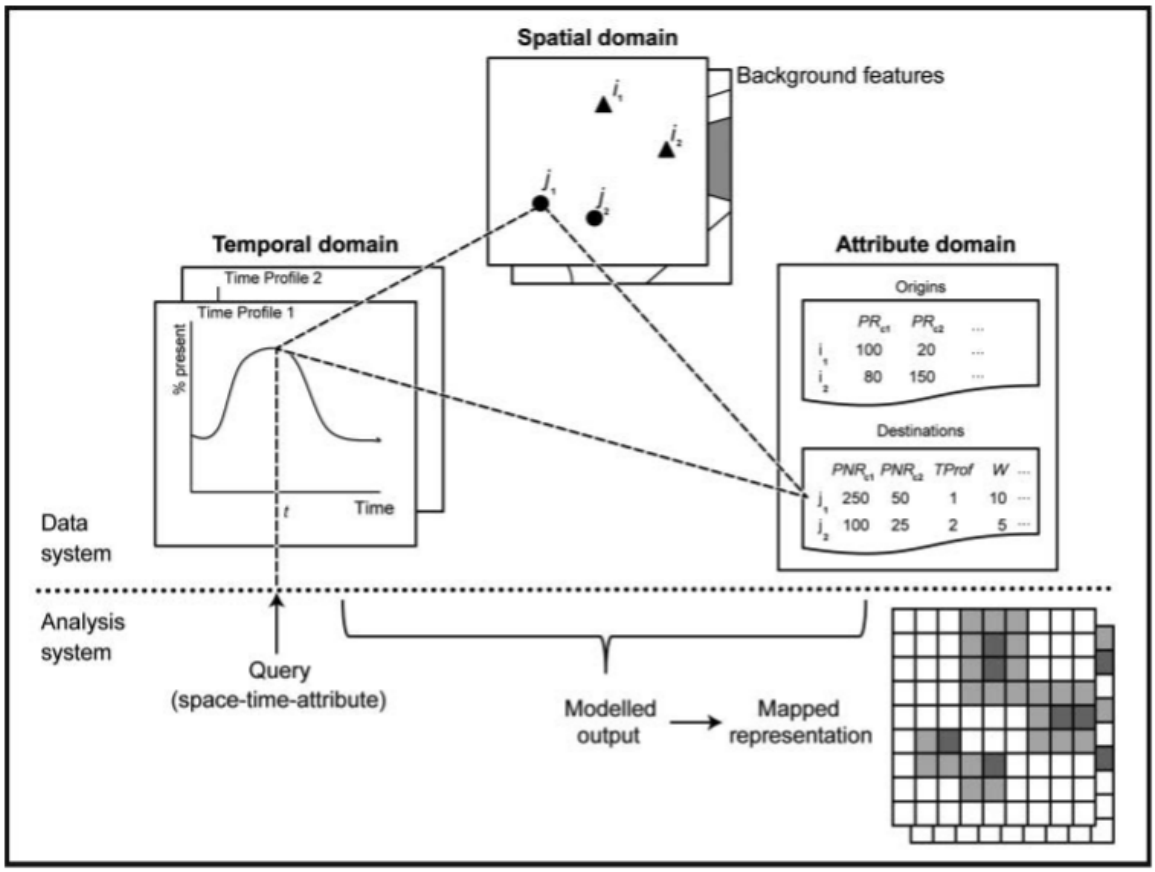

Figure 4: Framework for spatiotemporal population modeling (Martin et al., 2015).

A diagrammatic representation of the framework in use which includes both a data and an analysis system can be seen in Figure 4 separated by a dotted line. The data system provides a structure to display all spatiotemporal objects of interest whereas the analytical system provides the ability to answer specific queries using these data. There are three domains within the data system. Firstly, the spatial domain makes use of spatial containers of human activity (Ahola et al., 2007; Hagerstrand, 1970) denoted by *i, j,* and *k* in Equation 4 and shown as i_1, i_2, j_1, and j_2 in Figure 4. These containers could come in a range of sizes from individual buildings to census zones and are georeferenced by boundaries or point coordinates. There are "Origin" containers that house all PR in an area, the sum of which represents the entire modelled population. Additional "Destination" containers are locations populated solely by PNR such as offices, education, leisure, and healthcare facilities. A background feature layer (indicated by a second overlapped layer in Figure 4) provides the likely spatial distribution of the PT in between containers by including transportation links and land use classes that cannot contain any population like open water or inaccessible areas.

The second domain relates to the temporal characteristics of the system and is perhaps the hardest to model. As suggested by Ahola et al. (2007), temporal understanding of the population can only be obtained by collecting the details of hourly and daily activities which is not a complete record of population movement but is instead a set of observations and assumptions. In order to improve the fidelity of risk maps generated by Pilko et al. (2022), each spatial container was allocated multiple time profiles describing the proportion of the population present in regard to the total population over time. Previously, a single time profile

was assumed for the whole population based on NHAPS data found in Klepeis et al. (2001). The updated software encompasses a wider number of time profiles taken from a range of 2011 data which can be found in Appendix 1. With a sufficient amount of information available, different profiles could be used to describe the same location with more detail and accuracy.

Lastly, the third domain of the data system holds the attributes of the spatial containers from the first domain. It can be identified that different subgroups of the population will exhibit various patterns throughout the day which limits their mobility between locations. For example, children at various ages could be assumed immobile during school hours on weekdays as their movements within that period of time would be restricted to a single location. As such, each destination containers have associated catchments alongside different time profiles which represent the area where origin populations could be drawn towards to participate in activities. These catchments can take a variety of forms and it provides the interaction weights $w_{i,j,t}$ in Equation 4 and is simplified in Figure 4 as column *W*.

Moving on to the output system which relates to the spatiotemporal analysis of the data system, the analysis begins by the user's request of a spatiotemporal query in which results of a study area comprising of a specific number of analysis units at time *t* is to be found. Equation 4 summarises the estimated population distribution for each container at a specific time across the spatial, temporal, and attribute domains. The population is then reallocated from origin to destination containers based on the interaction weights which can be found via catchment areas or to match known proportions of PT from successive distance bands such as those recorded in travel-to-work data (Martin et al., 2015). The aggregated result can then be explored in a variety of forms including statistical analyses, data tabulations, and mapped representations.

4.2 Fatality Risk Estimation

Once the estimated population distribution of an area is generated, the data is converted to a GeoTIFF to aid in visual interpretation and Geographic Information System (GIS) applications. A Tagged Image File Format (TIFF) is a method of storing raster graphic images while a GeoTIFF is a public domain metadata standard which allows georeferencing information to be embedded within the image itself (OmniSci, 2021). Essentially, every pixel on a GeoTIFF is able to provide the geocoordinates of the cell and the associated value within it corresponds to the estimated population number of the container. This value can subsequently be used to plot a raster map made out of "gridded" data as seen in Figure 5.

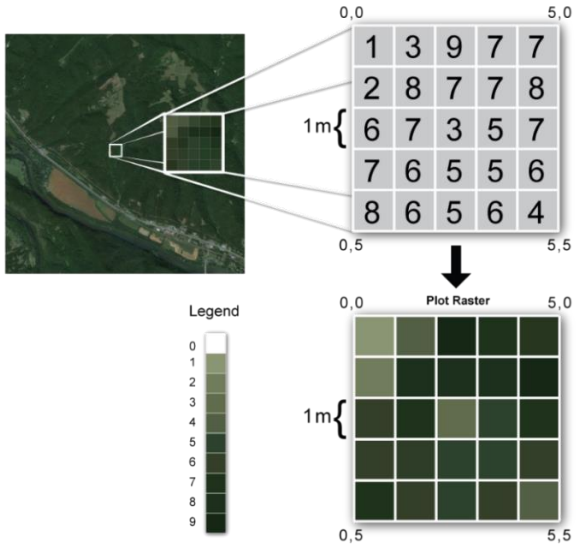

Figure 5: Example of a GeoTIFF raster map. Each pixel represents an area on the Earth's surface with an associated colour bar to visually represent the values within each pixel (Wasser et al., 2021).

Notice that this is similar to the risk maps introduced in Figure 3. Using Equations 1 to 3 from Section 1.5 allows the generation of fatality risk maps from raster data. The resulting resolution of the risk map depends on the spatial resolution of the raster data which is the size of each pixel. As the primary data source (Martin et al., 2021) used in this paper has fixed a spatial resolution of 200 metres due to its nature of being a general-purpose demonstrator, its raster data will have to be upsampled in order to provide the required resolution for comparison with Pilko et al. (2022). It is possible for the framework set out above to accommodate more detailed locational references for some elements of the population distribution, but this would require further estimations of the spatial distributions of different population sub-groups which will greatly increase computation times. As such, the upsampling of output data would be sufficient in providing a low computation "proof of concept" for this approach.

Upsampling is the process of inserting zero-valued samples between original samples and it is associated with the process of resampling multi-rate digital signals. It can be synonymous with the term "expansion", or it can also describe the entire process of expansion and filtering (Oppenheim et al., 1999). In the case of raster data, when upsampling is performed on a gridded dataset, it produces an approximation of the raster map that would have been obtained by sampling at a higher resolution. There are multiple ways to resample raster data, but the remainder of this section will only be focused on upsampling by an integer factor followed by a bilinear interpolation method. In the expansion phase, a new sequence comprising of the original samples separated by $L-1$ zeros where L is the integer factor is created (Harris, 2004):

$$x_L[n] = x[n]_{\uparrow L} \tag{5}$$

The discontinuities between grid values can then be smoothed out via bilinear interpolation which replaces the zeros. This is done by taking the weighted average of the four neighbouring grid cells to generate a new value.

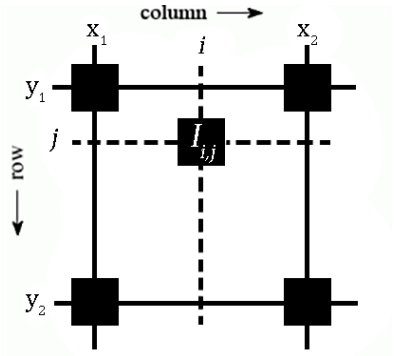

Figure 6: General representation of bilinear interpolation.

Depending on L, there would be $L-1$ number of new cells in between each columnar and row grid cells respectively. From Figure 6, the intensity, $I_{i,j}$ of a cell with position i, j with respect to existing samples can then be interpolated using two linear interpolations (hence the term "bilinear"). This is first achieved by linearly interpolating between the values at column x_1 and x_2 on each row y_1 and y_2 which gives

$$I_{iy_1} = \frac{x_2 - i}{x_2 - x_1} \cdot I_{x_1 y_1} + \frac{i - x_1}{x_2 - x_1} \cdot I_{x_2 y_1} \tag{6}$$

$$I_{iy_2} = \frac{x_2 - i}{x_2 - x_1} \cdot I_{x_1 y_2} + \frac{i - x_1}{x_2 - x_1} \cdot I_{x_2 y_2} \tag{7}$$

and then interpolating linearly once more between these values:

$$I_{ij} = \frac{y_2 - j}{y_2 - y_1} \cdot I_{iy_1} + \frac{j - y_1}{y_2 - y_1} \cdot I_{iy_2} \tag{8}$$

5 Results & Discussion

The software discussed in Section 2 was developed in Python using data science and geospatial libraries with visualisation based on the Holoviews library. Geocoordinates obtained from Population24/7 uses EPSG:27700 which was converted to Pseudo-Mercator (EPSG:3857) in order to match the tile projection of Open Street Map's (OSM) webservice.

5.1 Implementation

For the initial case study, a 15 by 15 km region of the city of Southampton and its surrounding area was used with a 5 km buffer zone in the simulation to avoid edge effects from major spatial containers that could be located outside the analysis area yet interact with the population number within through overlapping transits to work or service catchment areas. A satellite view of the region can be seen in Figure 7.

Bounding Coordinates:

Corner	Latitude	Longitude
Top-Left	50.99720	-1.52538
Top-Right	50.99720	-1.31190
Bottom-Left	50.86154	-1.52538
Bottom-Right	50.86154	-1.31190

Figure 7: City of Southampton and its surrounding area used in the case study (Google Maps, 2022).

To model the population, origin containers made use of 2011 census data. Potential destinations in which human activity can be expected to congregate includes accommodation, agriculture, fishing, education, healthcare, transportation networks, public spaces, office blocks, retail areas, the arts, and the service sector. The population was divided into seven sub-groups based on age as it was easier to estimate temporal variations from data sources using these categories. Results from each sub-group was then summed together to produce the distribution of the total population. The age range of each sub-group can be seen below:

- 0 – 4
- 5 – 9
- 10 – 15
- 16 – 17
- 18 – 64HE (population members who are undertaking higher education studies)
- 18 – 64NSTU ("non-student" population members)
- OV65 (population members above the age of 65)

Time profiles and starting population counts for origin containers assumed that school term times are currently in session. As such, the results from this case study will not be relevant for out-of-term periods like the summer holidays where students do not go to school, and a major transit factor of incoming and outgoing tourists would have to be accounted for. The

exact date of the model was 17th October 2011 to investigate a regular term-time Monday. Data was generated with temporal intervals of one hour between 12 am and 11 pm. The resulting raster output was then upsampled with bilinear interpolation as there is no distinct boundaries between data points and it smooths the output grid. An integer factor of 8 was also used to approximately match the resolution obtained in Pilko et al. (2022). This value was found to be the most suitable as smaller integer factors reduces the accuracy of results while higher values exponentially increase the computational time required.

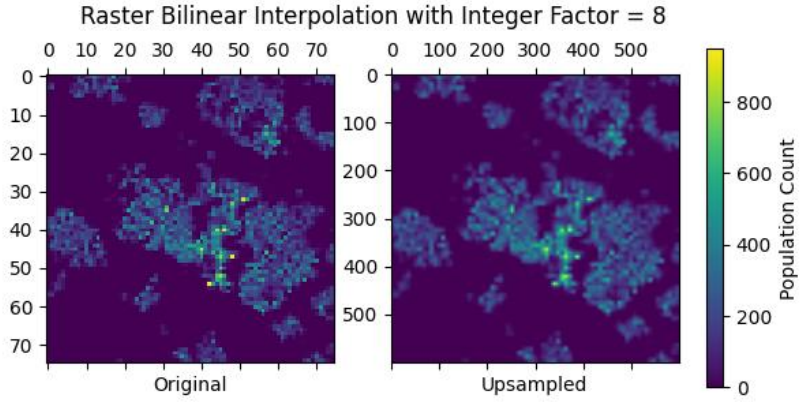

Figure 8: Comparison between upsampled and original data sample using integer factor expansion and bilinear interpolation. Resolution can be seen to increase from 75 × 75 to 600 × 600 number of grid cells.

The UAS used for fatality risk calculations was a Swoop Aero aircraft which is pictured in Figure 9. It is a small, fixed wing UAS capable of vertical take-off and landing (VTOL) and is suitable for transporting small payloads. Currently, the Swoop Aero is undergoing logistics trials in the UK for the National Health Service (NHS) to assess the feasibility of transporting patient samples between hospitals with helipads (Kesteloo, 2021).

Table 1: Swoop Aero aircraft parameters used in study (Pilko et al., 2022).

Parameter	Value
Mass (kg)	17
Length (m)	1.63
Width (m)	2.22
Cruising Altitude (m)	100
Horizontal Airspeed (m/s)	31
Frontal Area (m^2)	0.5
Ballistic Descent Drag Coefficient	0.8
Glide Airspeed (m/s)	21
Glide Ratio	11
Event Probability (h^{-1})	5×10^{-3}

Figure 9: The Swoop Aero aircraft (JigSpace, 2020).

5.2 Results

5.2.1 Southampton City

Using Population 24/7 to generate the population dataset used in the Southampton case study gives a 75 × 75 raster as seen in Figure 10:

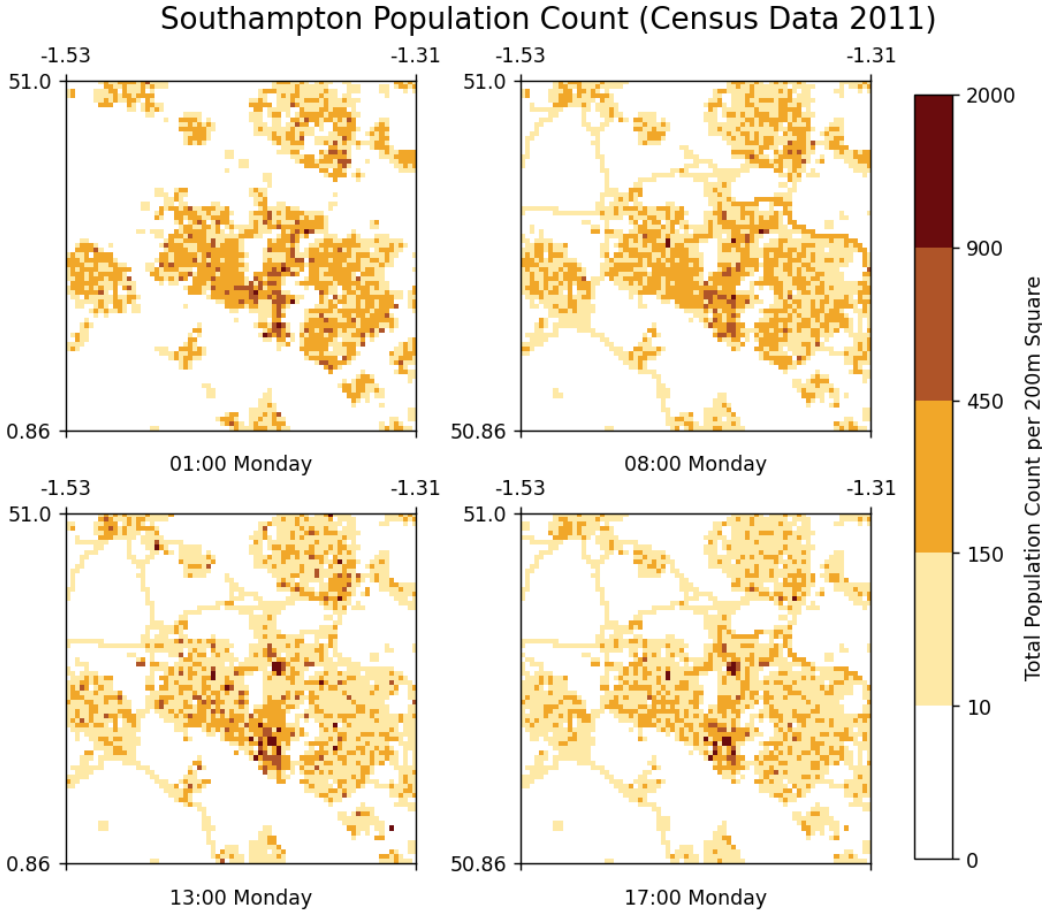

Figure 10: Population counts of Southampton, UK. and its surrounding areas at different times of day. A single cell correlates to a 200 m by 200 m region and all bounding coordinates are in decimal degrees.

The times of day in 24-hour format that are displayed in Figure 10 were chosen to match those in previous work conducted by Pilko et al. (2022) so that a suitable comparison can be made between the two methodologies. A non-linear colour scale was used to visually distinguish between different numbers of population members and it can be seen in the figure that the cells in white represent places in which there is a low density of people (such as a quiet highway at 1:00 a.m. in the morning) or areas that are unpopulated like the River Itchen and River Test that borders the southern tip of the city. Inversely, dark brown pixels show regions in which the model predicts heavy foot traffic at that time of day (a shopping district north of the tip as well as a university campus north-east of a large park at the center of the city).

The sample rate of the data was then increased via upsampling by a factor of 8 to produce a 600 × 600 raster which was fed into the SEEDPOD Ground Risk (Pilko and Tait, 2021) software to calculate the estimated strike and fatality risk a single UAS with flight parameters in Table 1 would have if it were to fly over a particular area. It does this by implementing the ground and fatality risk equations introduced in Section 3 and 4 to each cell within the raster. It can also be seen in Figure 11 that the bilinear interpolation used during upsampling have smoothed the raster to provide a more organic shape and in Figure 12 the places in which the two sources of data differ.

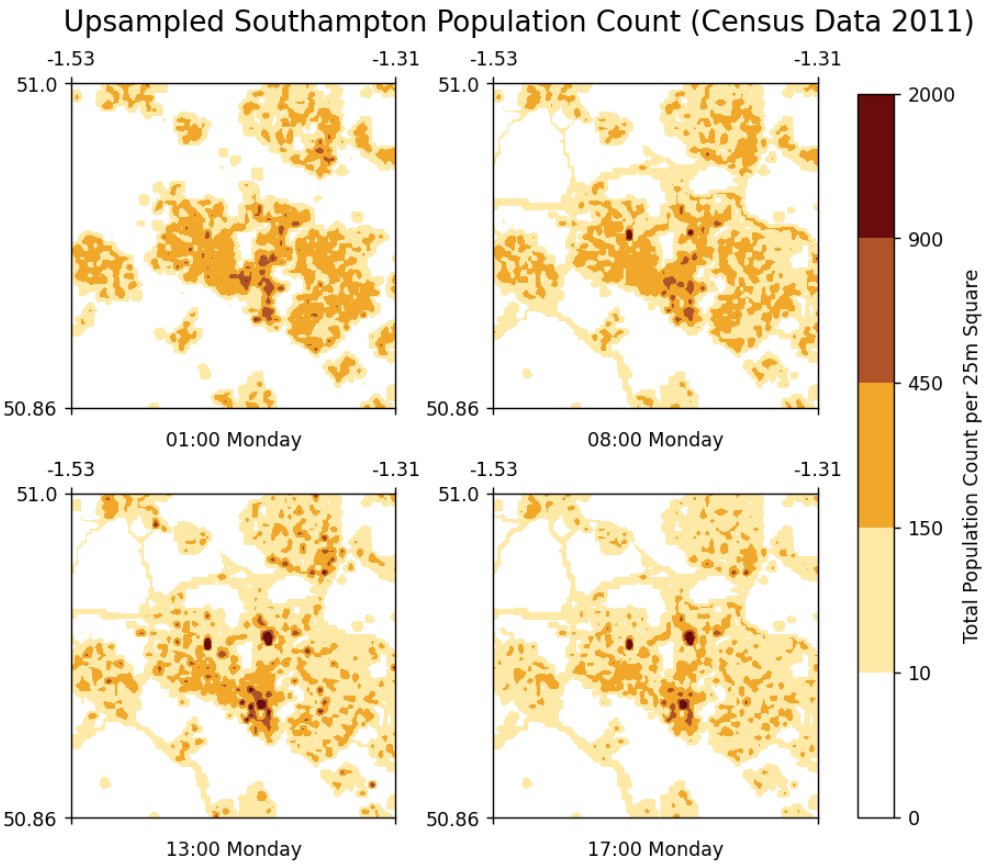

Figure 11: Upsampled population counts of Southampton, UK. and its surrounding areas at different times of day. A single cell correlates to a 25 m by 25 m region and all bounding coordinates are in decimal degrees.

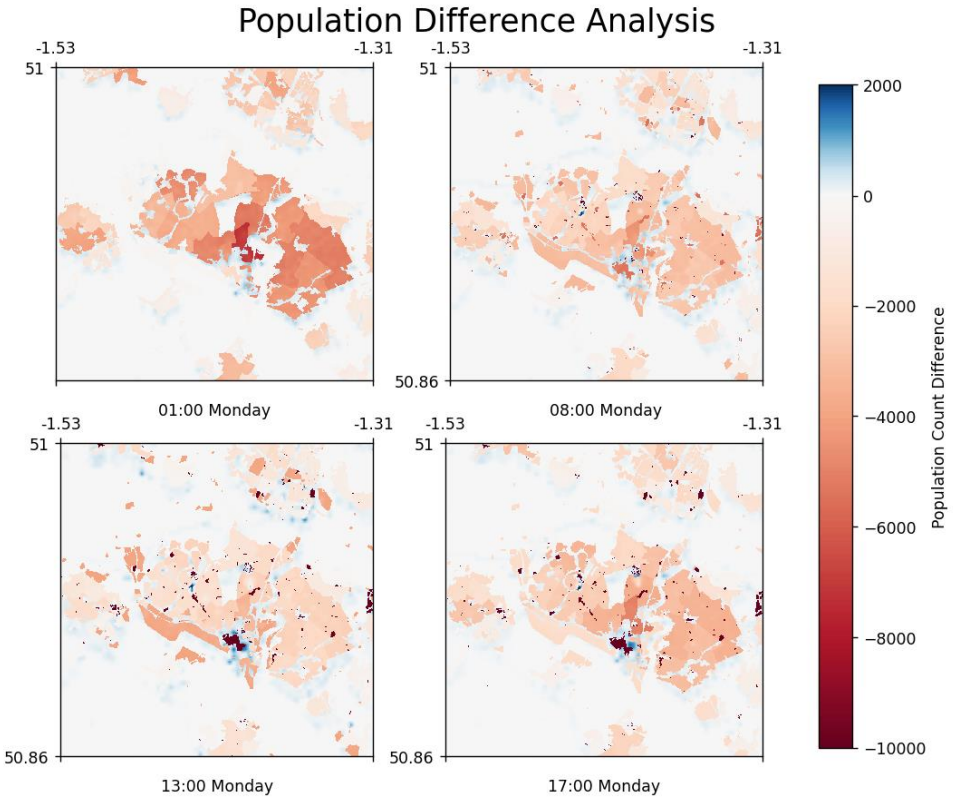

Figure 12: Difference in population counts between 2011 Census and 2001 NHAPS data during different times of the day for the Swoop Aero UAS. All bounding coordinates are in decimal degrees.

Only a single UAS was used to generate the strike and fatality risk maps as this demonstrates the changes in risk due to varying population density and time, not from aircraft parameters. Figures 13 and 14 displays the potential strike and fatality risk of a person differing with time. It can be seen that the heatmaps of both figures are similar which was expected as they share the same input, but the risk values are different due to additional considerations such as the shelter factor and impact energy used when estimating the probability of fatality during a UAS strike. In this example, it was found that the risk of fatality was roughly lesser than the risk of being struck by a single order of magnitude.

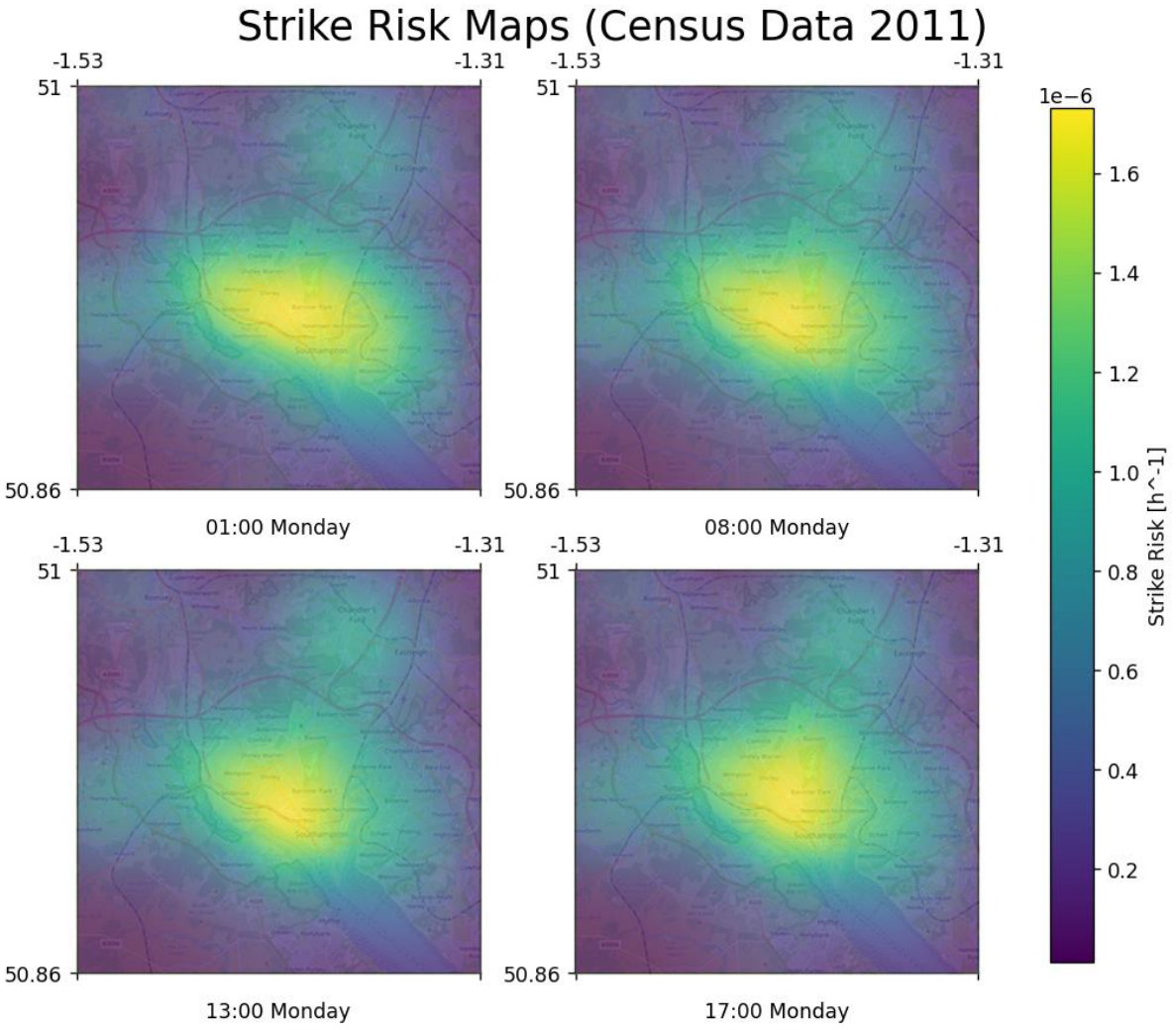

Figure 13: Comparison of strike risk maps around Southampton, UK. during different times of the day for the Swoop Aero UAS. All bounding coordinates are in decimal degrees.

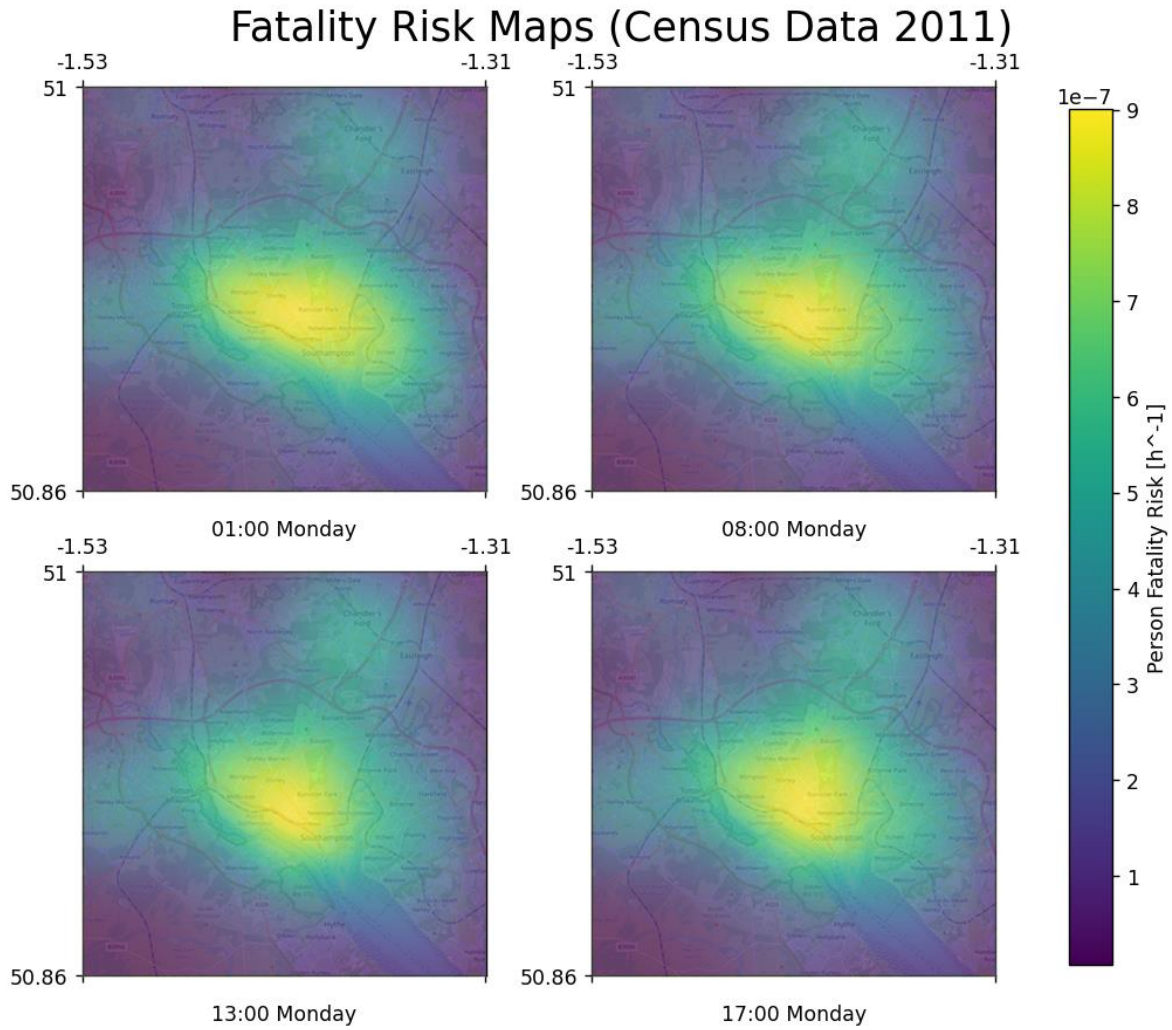

Figure 14: Comparison of fatality risk maps around Southampton, UK. during different times of the day for the Swoop Aero UAS. All bounding coordinates are in decimal degrees. It can be noted here that the colour scale used to map fatality risk is ten times smaller than that of the strike risk.

A difference raster was then created by subtracting one raster from another. The resulting image gives a comparison of the cell values between both datasets. In Figure 15 and 16, a pixel leaning towards the blue spectrum indicates that the risk value estimated with inputs from Census 2011 data was higher than NHAPS 2001 whereas cells with an increasingly red intensity means a higher reduction of said risk. It can also be seen that the difference of fatality risk fluctuates more than the strike risk and for both examples the time in which there was the least amount of difference between the two samples was 5:00 p.m. in the evening.

Figure 17 plots the average strike and fatality risk over a regular Monday so that an easier comparison could be made. As seen in the diagram, apart from the census data estimating an overall reduction in risk, its risk values also fluctuated more noticeably throughout a 24-hour period. This could be attributed to the temporal modelling of the current methodology giving a more dynamical representation of the population and hence greater output variation. Lastly, a Theta* pathfinding algorithm which uses weighted graphs to find a least cost path from a starting node to a termination criterion (Daniel et al., 2010) was used to produce Figure 18. This method was chosen due to its easy implementation and ability to skip in-between nodes to give a shorter (though not a guaranteed shortest) path as compared to other variants of the A* search algorithm. It also creates simple and straight routes suitable for feeding into a UAS's onboard flight computer so that relatively low-risk flightpaths could be generated from these maps.

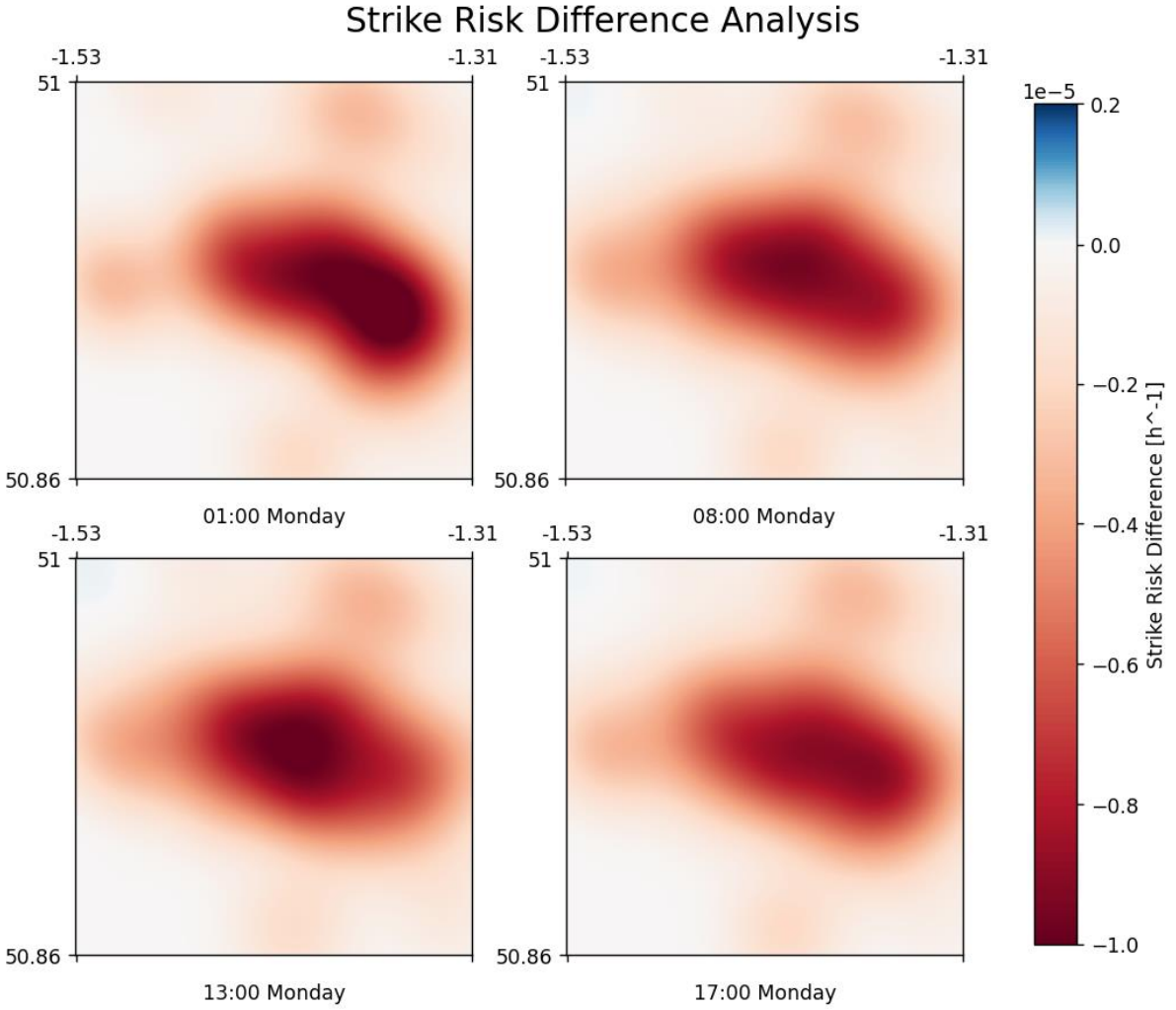

Figure 15: Difference in strike risk values between 2011 Census and 2001 NHAPS data during different times of the day for the Swoop Aero UAS. All bounding coordinates are in decimal degrees.

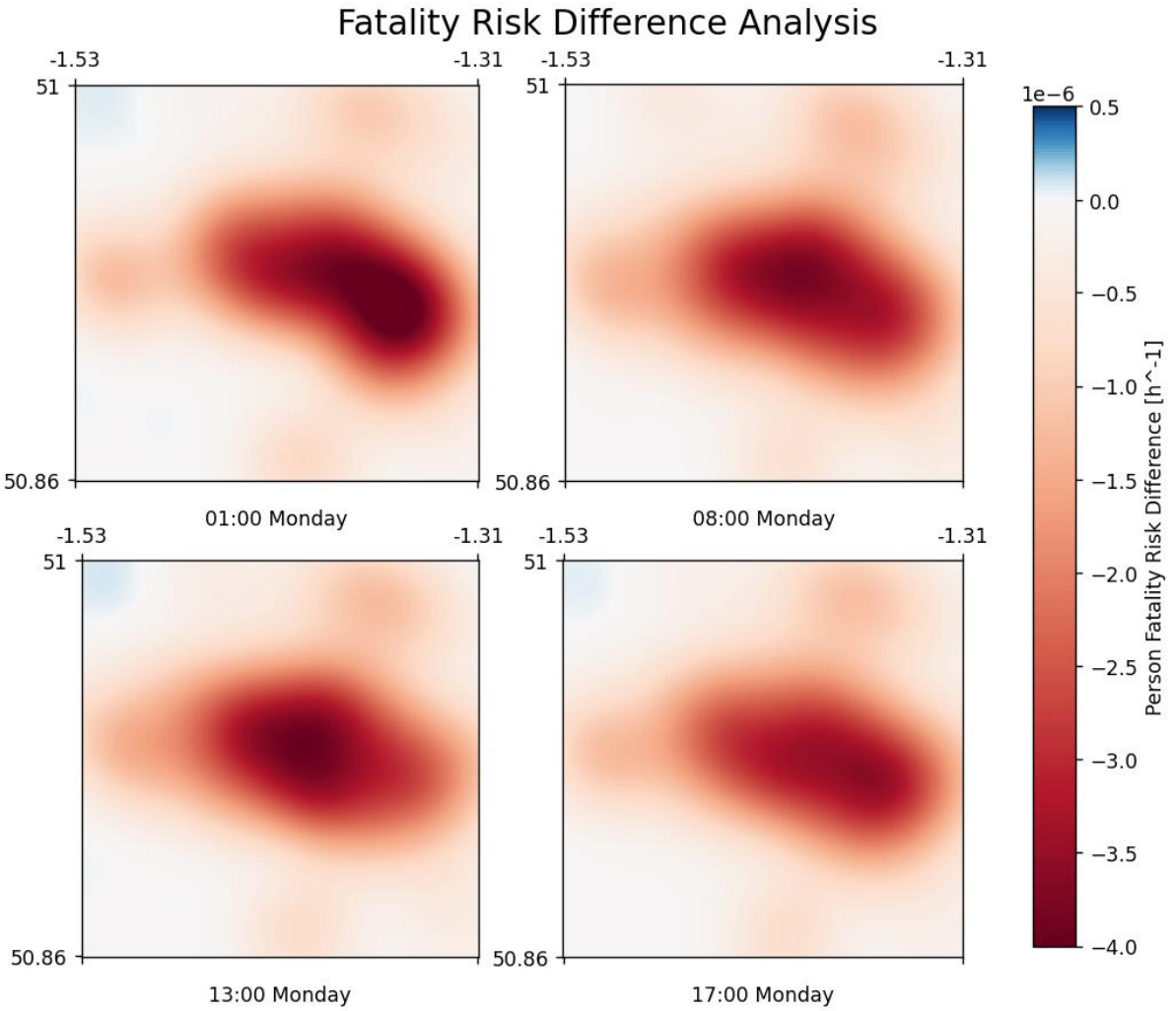

Figure 16: Difference in fatality risk values between 2011 Census and 2001 NHAPS data during different times of the day for the Swoop Aero UAS. All bounding coordinates are in decimal degrees.

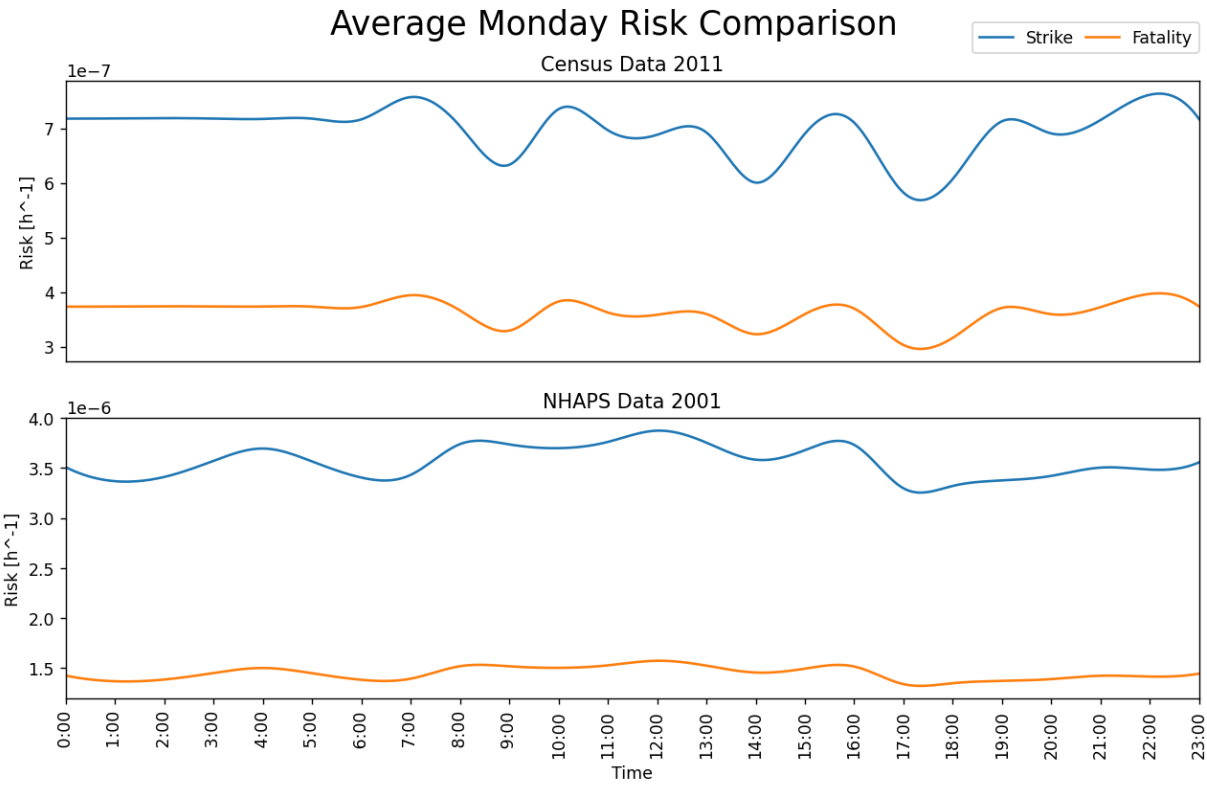

Figure 17: Average risk comparison between 2011 Census and 2001 NHAPS data during a normal Monday for the Swoop Aero UAS. Strike and fatality risk are plotted in blue and orange respectively.

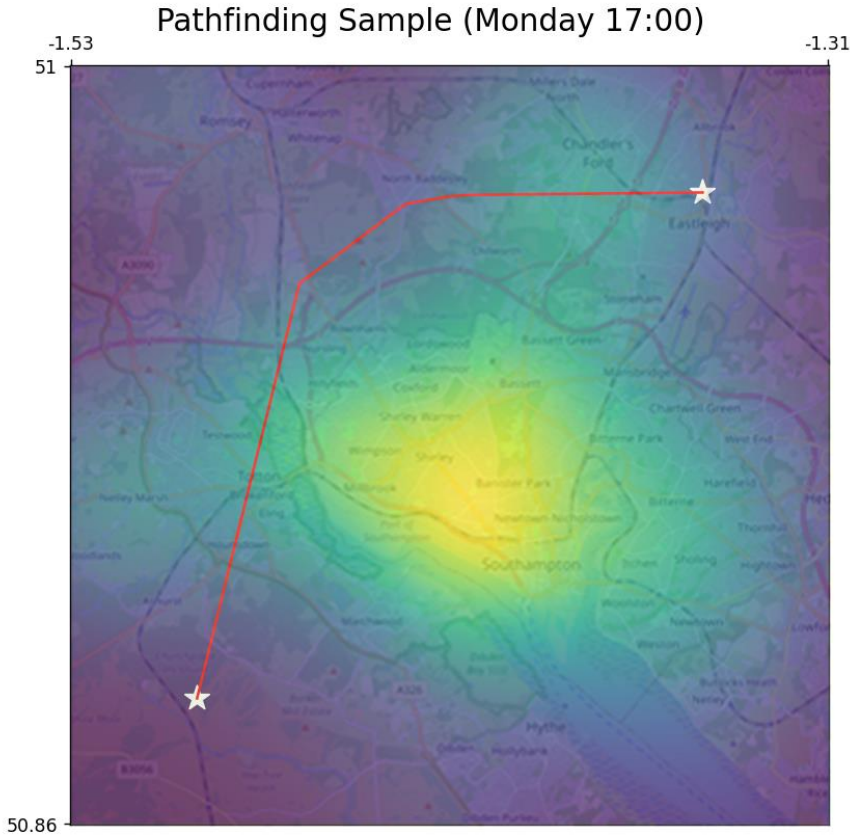

Figure 18: An example of Theta pathfinding implementation on a fatality risk map. White stars indicate start/end points, and the computed path is traced in red. All bounding coordinates are in decimal degrees.*

5.2.2 Hampshire County

As a test for this higher fidelity ground risk model, the software was then applied over the wider Hampshire County located in Southeast England. Current plans of establishing a UAS logistic network in this region is mainly focused on the rapid delivery of patient samples between medical centres. Seven surgeries were identified as potential candidates for trial runs, the details of which can be seen below:

Table 2: Details of candidate surgeries for UAS delivery trials.

Marker	Name	Post Code
1	Bishops Waltham Surgery	SO32 1GR
2	Cornerways Medical Centre	BH24 1SD
3	Diabetes Service Lyndhurst	SO43 7NG
4	Fordingbridge Surgery	SP6 1RS
5	Lymington Hospital	SO41 8QD
6	St Clements Surgery	SO23 8AD
7	TLC Romsey Hub	SO51 7QN

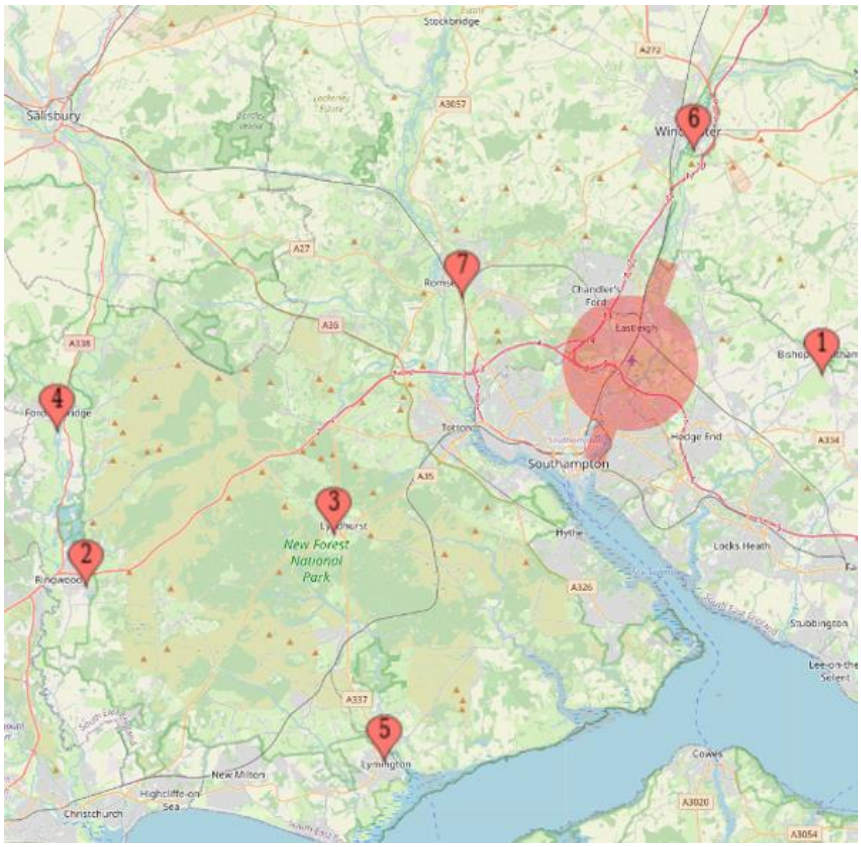

Bounding Coordinates:

Corner	Latitude	Longitude
Top-Left	51.13011	-1.84461
Top-Right	51.13011	-1.18896
Bottom-Left	50.71955	-1.84461
Bottom-Right	50.71955	-1.18896

Figure 19: Locations of candidate surgeries as seen on Open Street Maps. Red overlay indicates a Flight Restriction Zone (FRZ) around Southampton Airport.

The methodology outlined in Section 4 was repeated over this bigger area of approximately 46 by 46 km. Population count results from Population24/7 can be seen in Figure 20. The average fatality risk of the generated map was then computed and used as a threshold for a risk-distance compromise with a safety factor of 2 (half of the average value) which allows the algorithm to find the shortest path while ensuring that the maximum risk does not exceed a certain threshold.

For the example in Figure 21, Bishops Waltham Surgery was chosen as a "central hub" where all paths originated from. This is because its location is the nearest to Southampton and as such there isn't a direct and low-risk path to most of the other surgeries. Apart from the straight-forward routes to Lymington Hospital and St Clements Surgery, it can be seen that the first waypoint would bring the UAS away from the FRZ before circumnavigating the city via a corridor in-between Winchester and Eastleigh to reach its destinations. Sample collections would occur between 09:00 and 12:00, as well as 14:00 and 17:00, depending on the specific day of delivery and candidate surgery. Figures 21 and 22 shows the potential paths a UAS can take from Bishops Waltham Surgery to the other surgeries and the distance travelled with its associated fatality risk that the UAS would encounter respectively. This can then be compared with Figure 23 and its accompanying Table 3 displaying a comparison between the proposed UAS delivery paths against conventional road-based ones.

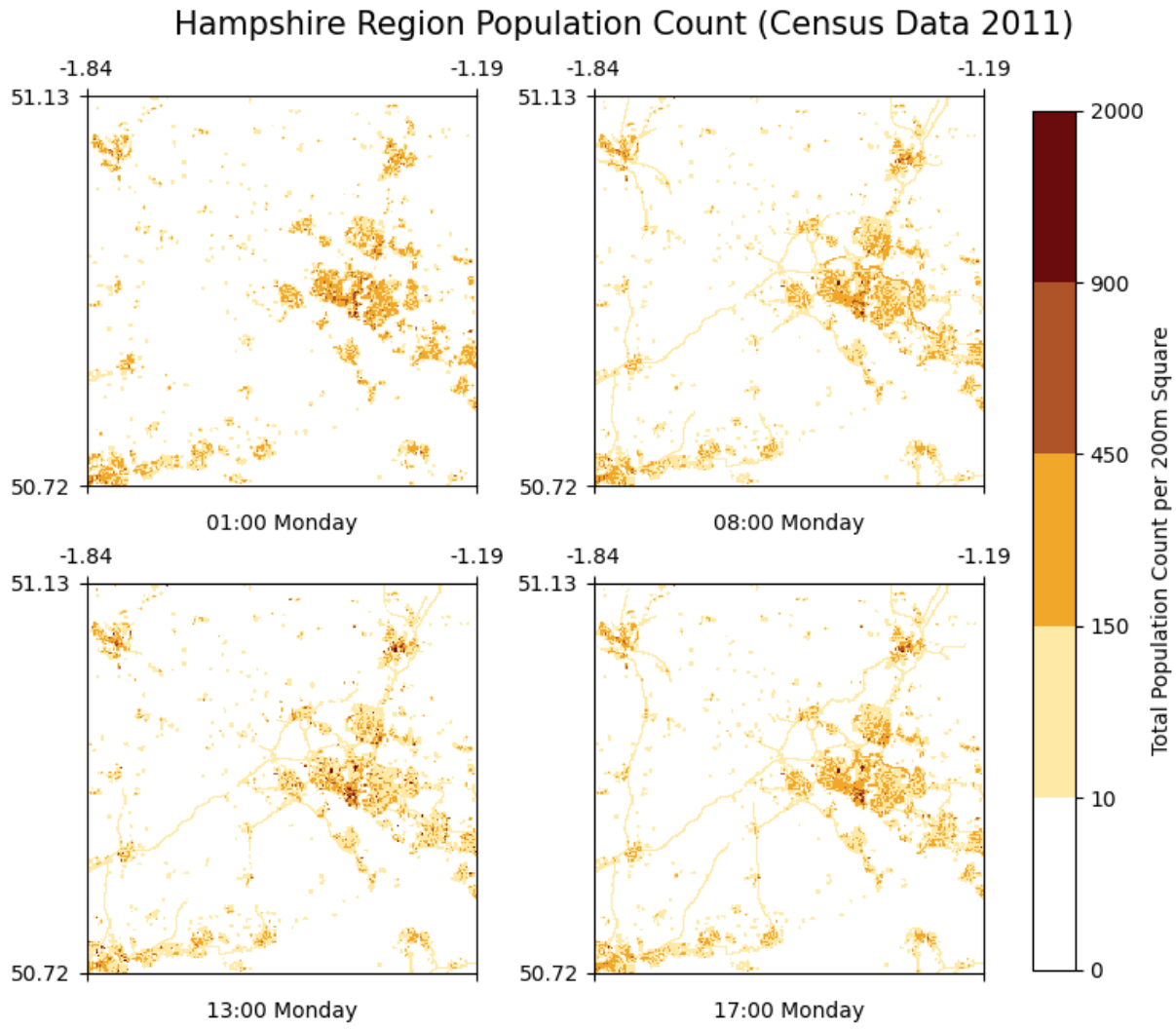

Figure 20: Population counts of a region within Hampshire County, UK. at different times of day. A single cell correlates to a 200 m by 200 m area and all bounding coordinates are in decimal degrees.

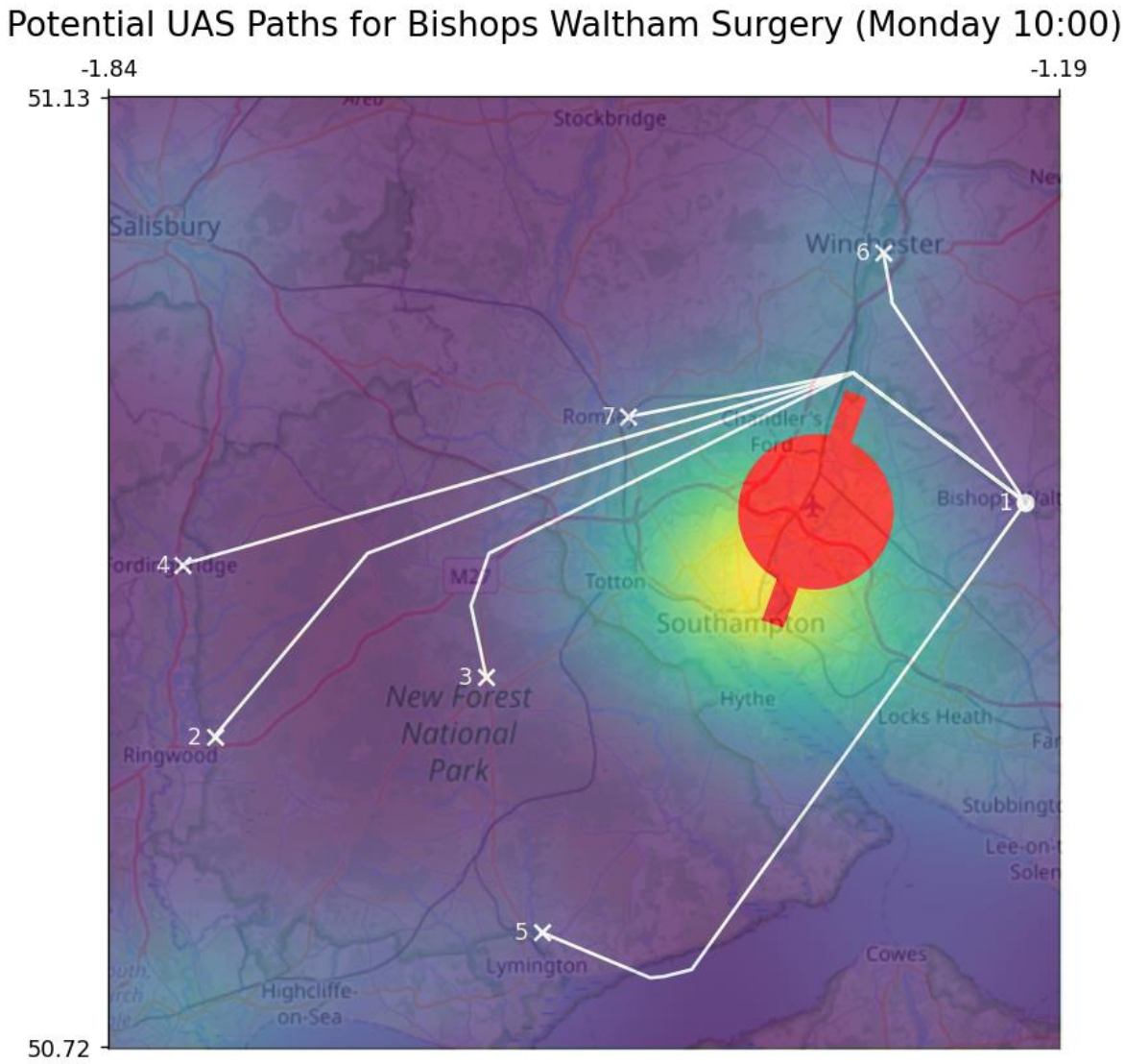

Figure 21: Potential paths a UAS can employ to deliver patient samples from Bishops Waltham Surgery (1) to other candidate surgeries (annotated with a white cross). All bounding coordinates are in decimal degrees.

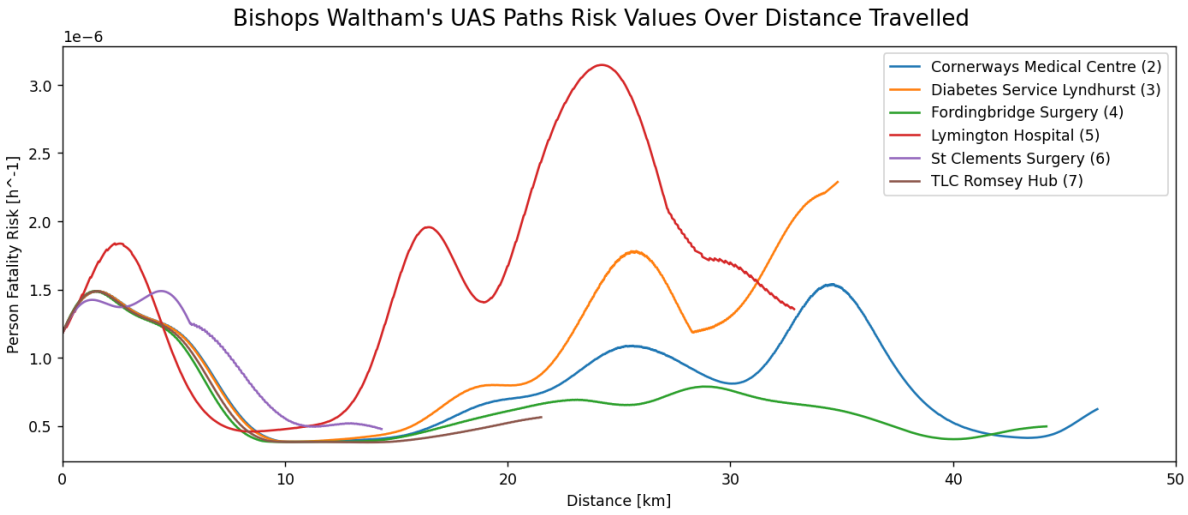

Figure 22: Plot of person fatality risk against the distance in which the UAS has travelled from Bishops Waltham Surgery to other candidate surgeries.

Table 3: Comparison of delivery distances/times between UAS and conventional road-based transport. Time estimates for vans were taken from Google Maps while UAS flight durations were calculated with the assumption that the Swoop Aero aircraft uses its horizontal flight speed from Table 1 throughout the entire path.

Marker	Destination	Distance (km)		Delivery Time (mins)	
		UAS	Van	UAS	Van
2	Cornerways Medical Centre	46.5	50.2	25	40
3	Diabetes Service Lyndhurst	34.8	39.5	19	35
4	Fordingbridge Surgery	44.2	51.8	24	48
5	Lymington Hospital	32.9	52	18	50
6	St Clements Surgery	14.3	16.7	8	19
7	TLC Romsey Hub	21.5	25.9	12	30

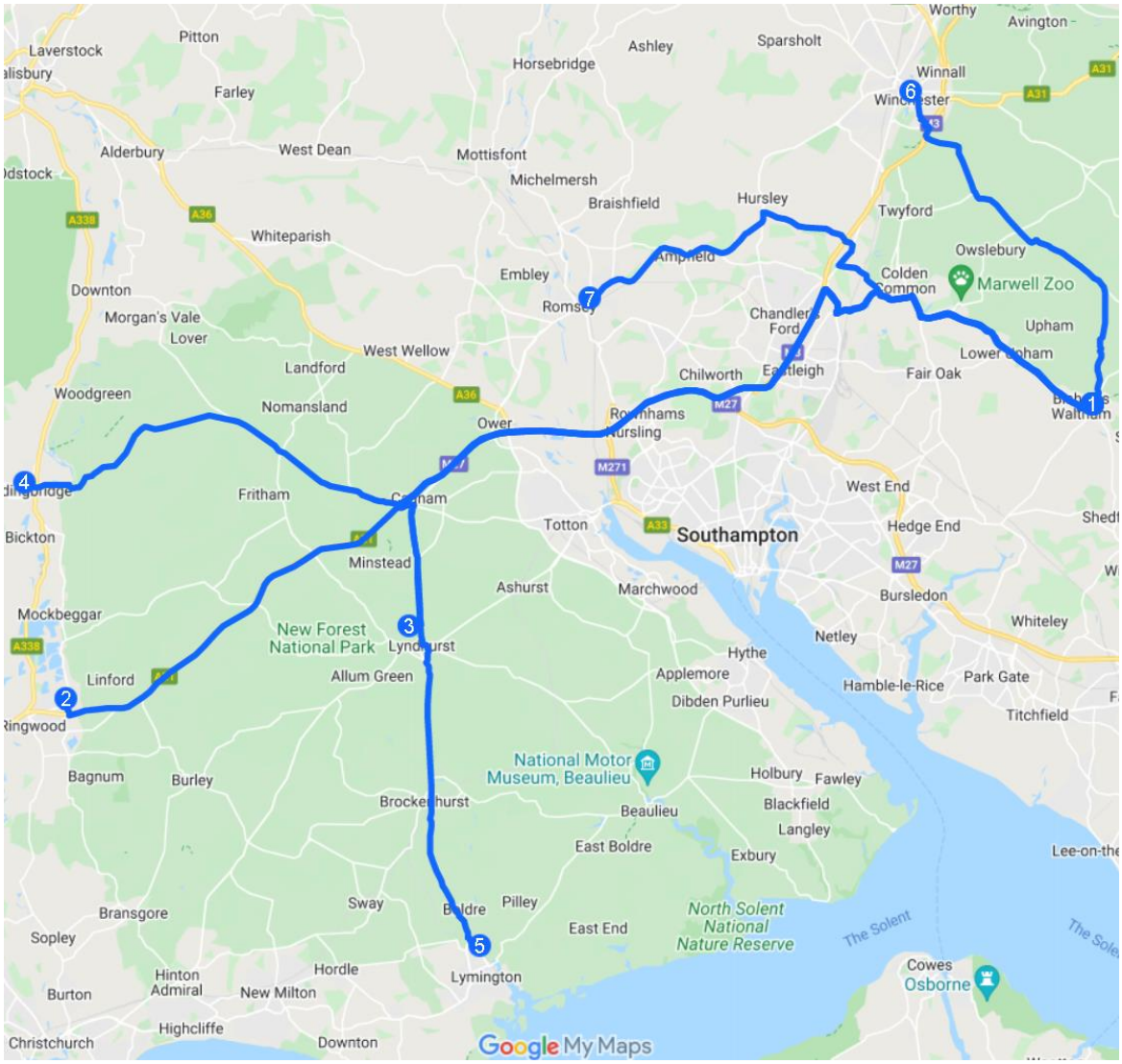

Figure 23: Potential paths a van would take to complete the same delivery (Google My Maps, 2022)

Expanding this methodology to other hours of the day to encompass all possible UAS delivery times for both the morning and evening sessions while allowing data continuity between them would yield all possible paths the UAS can take at any time. The average fatality risks and total risk value for these paths were then calculated to give Figure 24 with Figure 25 examining each individual total risk to show minute differences more clearly.

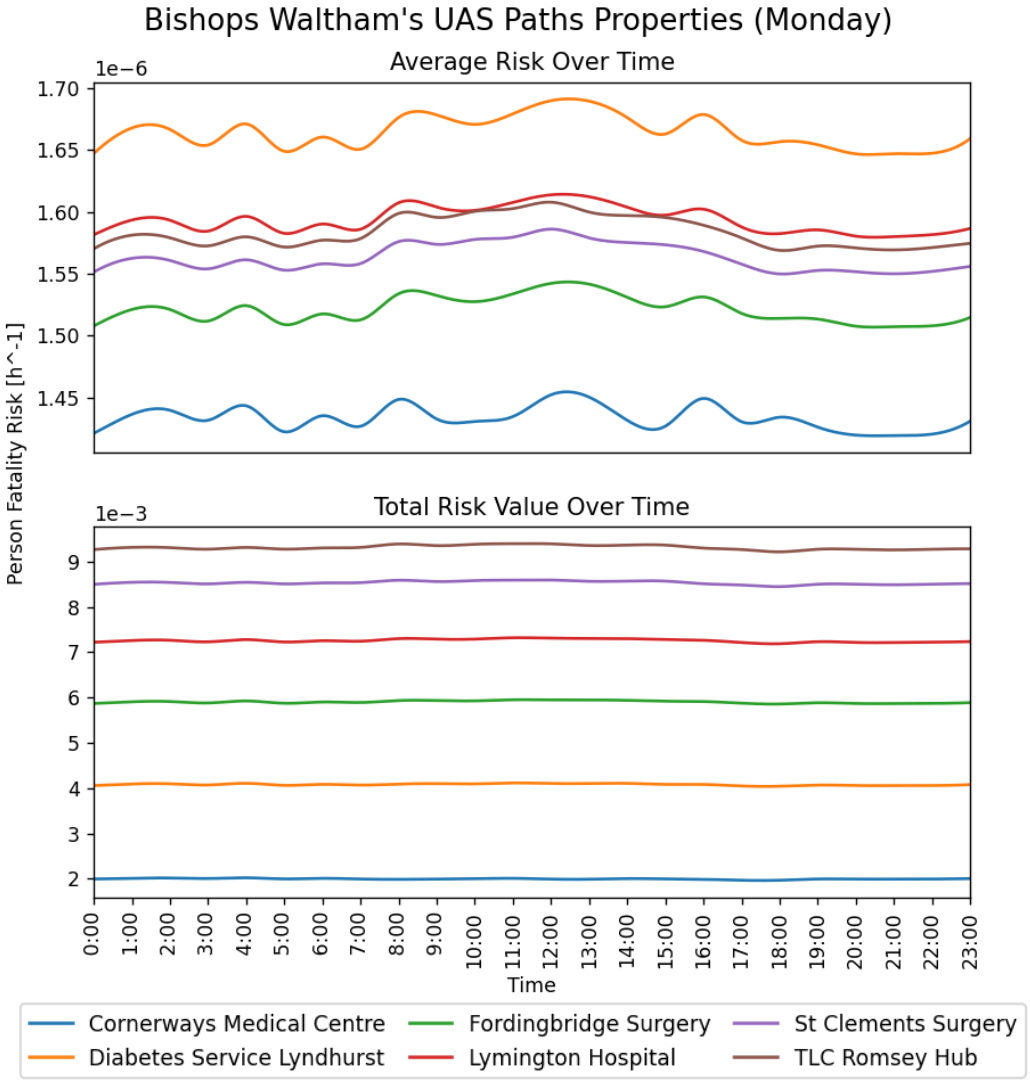

Figure 24: Plot of average and total fatality risk of UAS paths from Bishops Waltham Surgery to other candidate surgeries for specific hours during a regular term-time Monday.

From the figure above, it can be seen that the average fatality risk of a specific path does not fluctuate a lot throughout the investigated time period. However, paths taken to different candidate surgeries do have significantly different average risk from one another with the Cornerways Medical Centre and Diabetes Service Lyndhurst routes consistently having both the lowest and highest average risk respectively regardless of delivery hour. The total risk value was also plotted to show the accumulated fatality risk a UAS would experience while following a path. Instead of taking the average, this metric could be used to determine the best time for drone deliveries. As risk is cumulative (i.e., continuous UAS operation increases the probability of failure), it is best to avoid flying over high-risk regions altogether. As seen in Figure 25, taking the global minimum would mean that delaying sample collections to 18:00 would be best to minimise the risk of fatality for all locations whereas cancelling deliveries to Lymington Hospital, St Clements Surgery, and TLC Romsey Hub from Bishops Waltham Surgery altogether should be considered due to their consistently high total risk result.

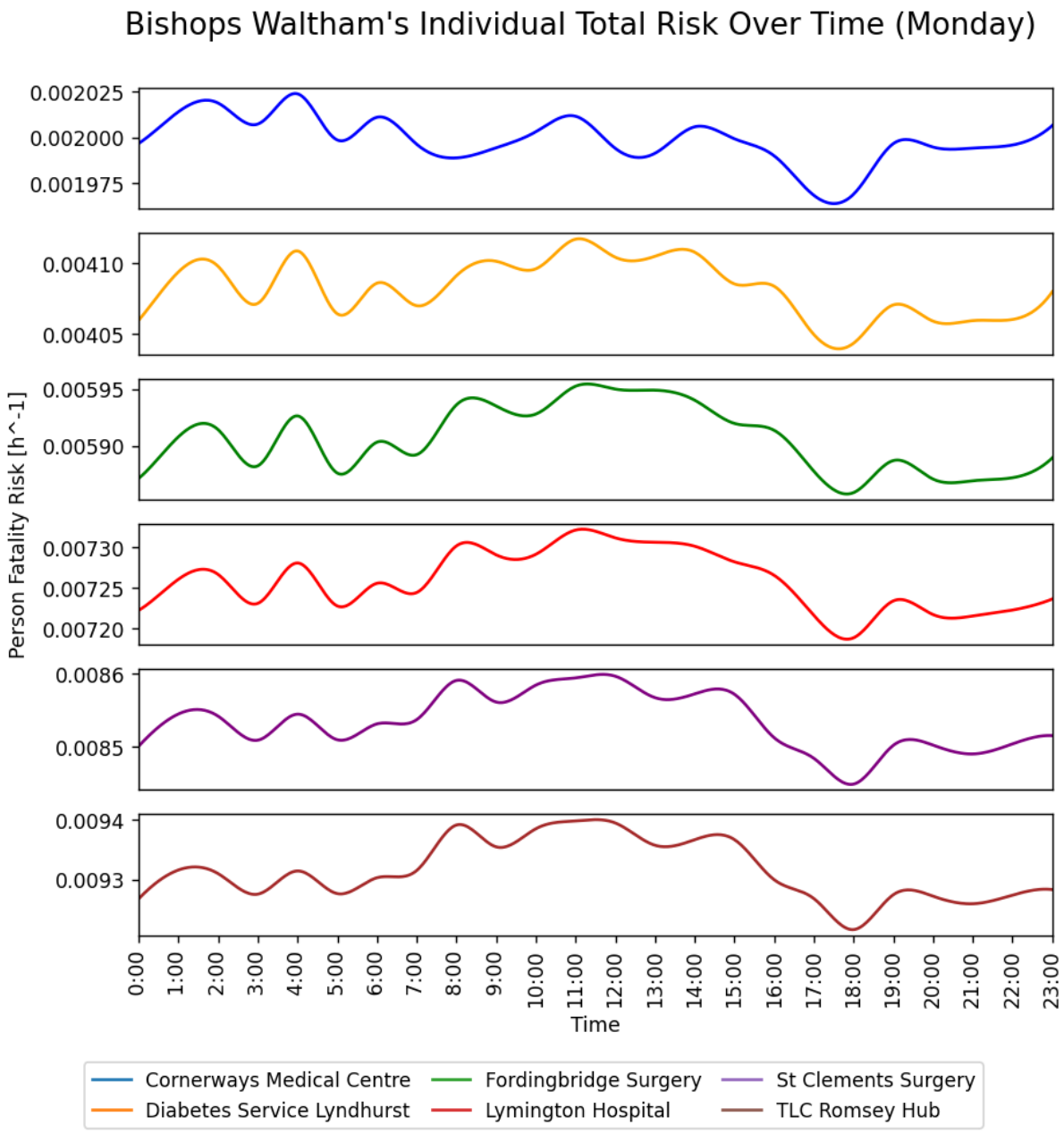

Figure 25: Expanded total risk over time plot.

5.2.3 Red and Green Practice to St Mary's Surgery

It was perhaps surprising that the risk values obtained in the previous case study fluctuated in a sinusoidal-like pattern as one would expect significant differences during various times of day (higher risk during peak footfall hours such as lunchtime and lower risk at night when the majority of the population is sheltered). This was not the case, however, and a likely explanation behind it could be due to the pathfinding algorithm consistently routing through areas with little to no risk and which also borders risk-dense regions. As such, the paths would occasionally clip the edges of these riskier zones whose risk changes probabilistically with time hence resulting in the sinusoidal output.

To determine whether this was the case, a final investigation was conducted using Blackfield's Red and Green Practice and St Mary's Surgery – two additional candidate surgeries with high sample outputs situated in highly populated areas separated by a body of water and away from any FRZs. Not only would their geographical position justify the use of UAS deliveries, but the lack of manoeuvrability to mitigate risk should also show how risk values actually fluctuate with respect to time. However, it should be noted that this route is likely not realistic due to the high levels of risk involved.

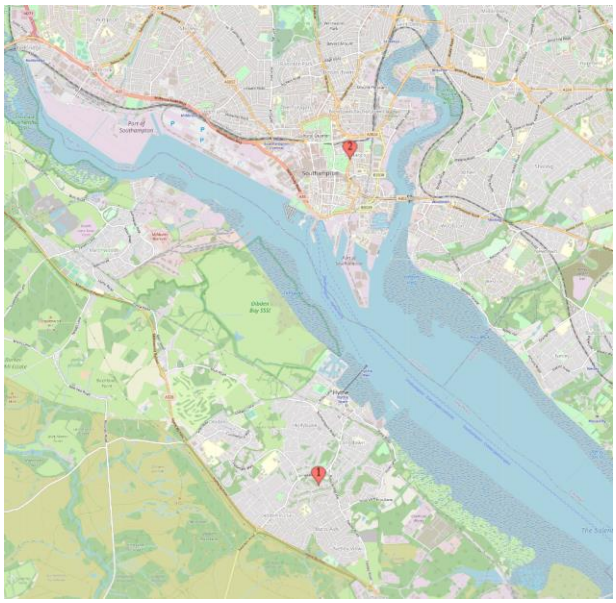

Bounding Coordinates:

Corner	Latitude	Longitude
Top-Left	50.92478	-1.47663
Top-Right	50.92478	-1.33915
Bottom-Left	50.84120	-1.47663
Bottom-Right	50.84120	-1.33915

Surgeries:

Marker	Name	Postcode
1	Red and Green Practice	SO45 5WX
2	St Mary's Surgery	SO14 1LT

Figure 26: Location of Blackfield's Red and Green Practice (1) as well as St Mary's Surgery (2) in Southampton's city centre as seen on Open Street Maps.

The same methodology was carried out as per the previous case studies and the resulting population count and fatality risk maps could be seen in Figure 27 and 28 respectively. It can also be seen that edge effects occur in the risk maps due to the low resolutions used in order to save computational time, but this can be ignored as we are only interested in the areas around the centre of the raster. As deduced previously, implementing the pathfinding algorithm produces a straight line (Figure 29) connecting both surgeries since the path have sufficiently high risk that the algorithm primarily minimises the distance as there is little difference in going around the long way through high-risk areas anyways. Figure 30 shows the resulting total risk over total distance travelled in red and the maximum fatality risk encountered during the flight in blue for different times of day. From here, it is much easier to determine the best UAS delivery times to minimise risk. The maximum risk increases from 6:00 a.m. onwards and fades out by 8:00 p.m. which lines up with the general day/night cycle where the majority of people are sheltered in their homes at night till early in the morning and are more at exposed during the day when they are travelling to school/work or are spending time outdoors.

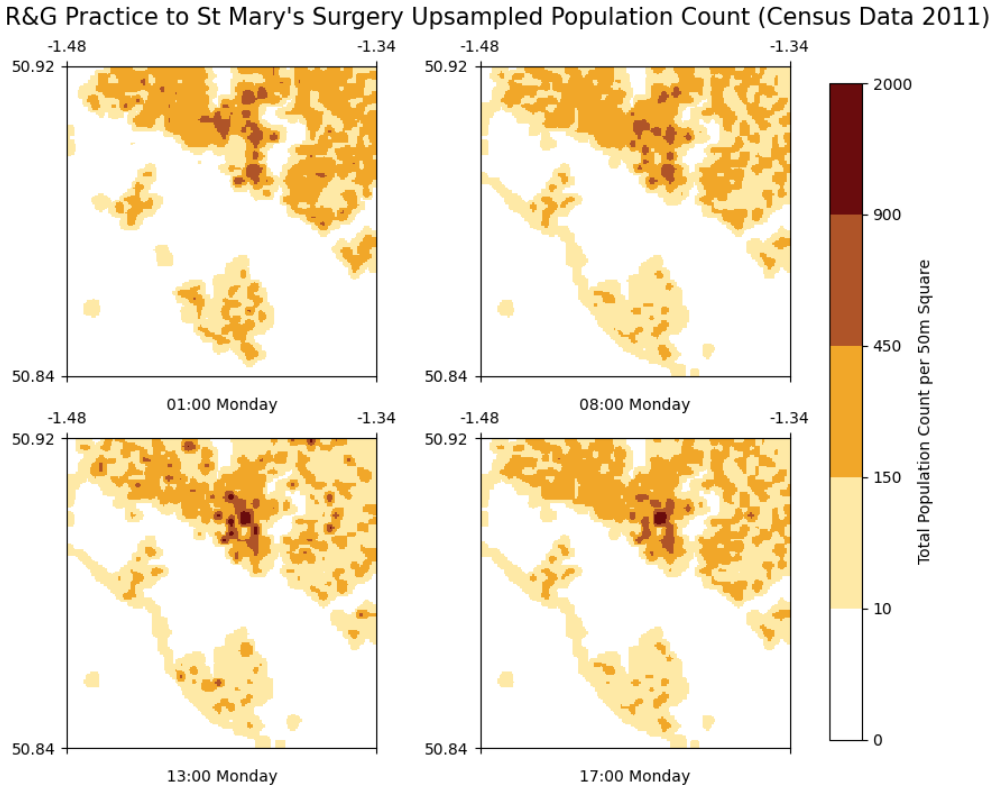

Figure 27: Population counts of a region south of Southampton, UK. at different times of day. A single cell correlates to a 50 m by 50 m area and all bounding coordinates are in decimal degrees.

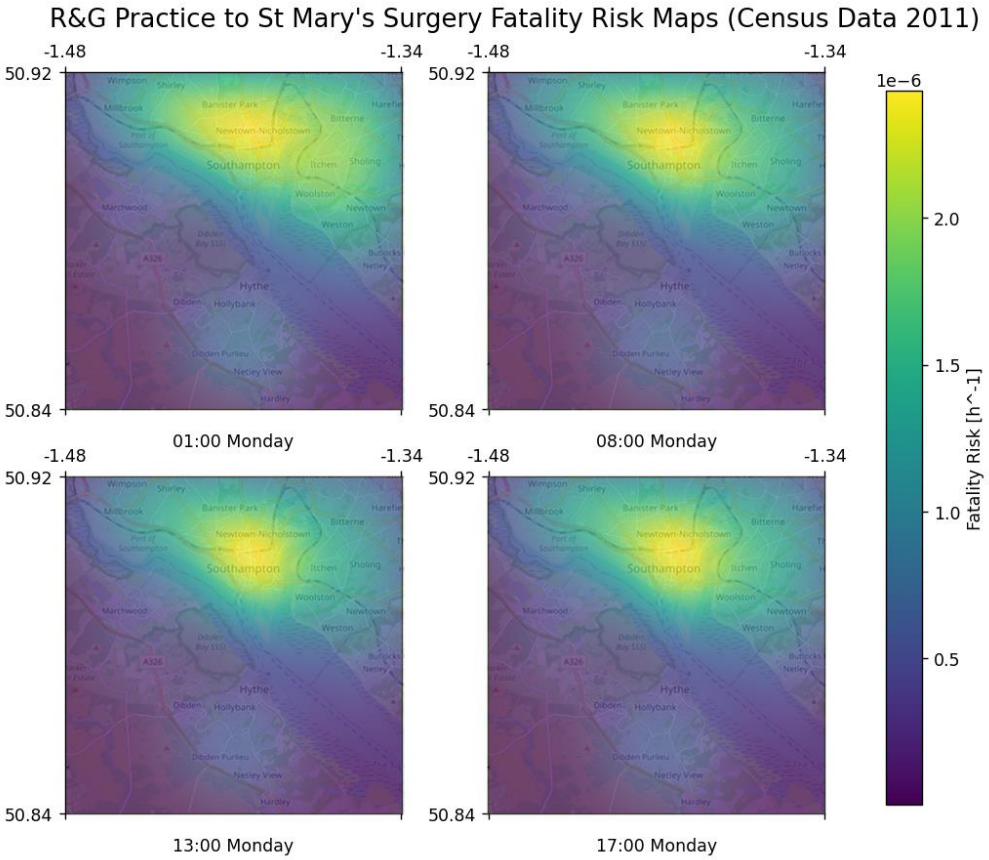

Figure 28: Comparison of fatality risk maps around Southampton's south, UK. during different times of the day for the Swoop Aero UAS. All bounding coordinates are in decimal degrees.

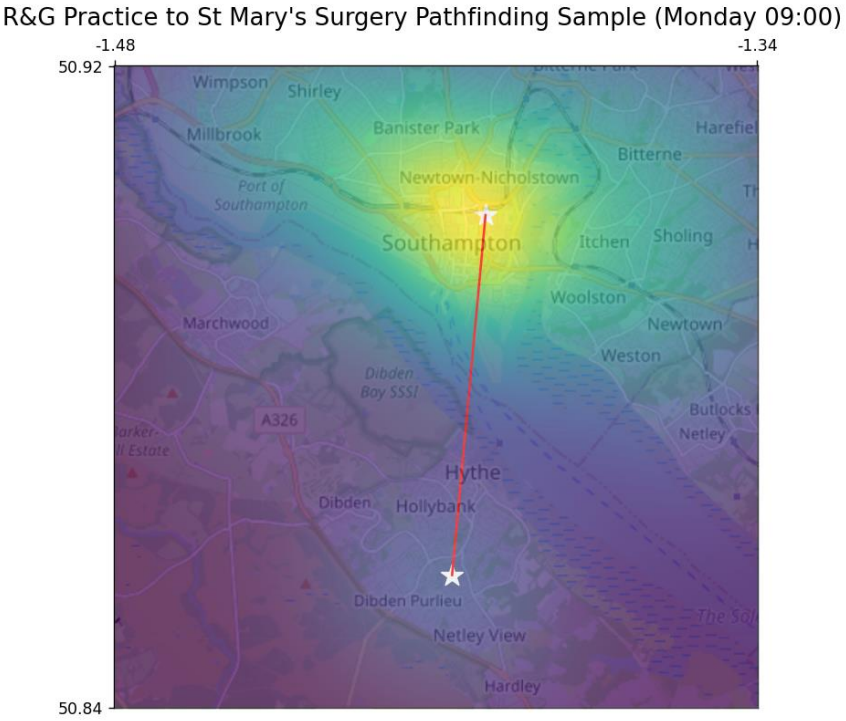

Figure 29: Singular path a UAS can employ to deliver patient samples from R&G Practice to St Mary's Surgery (both annotated with a white star). All bounding coordinates are in decimal degrees.

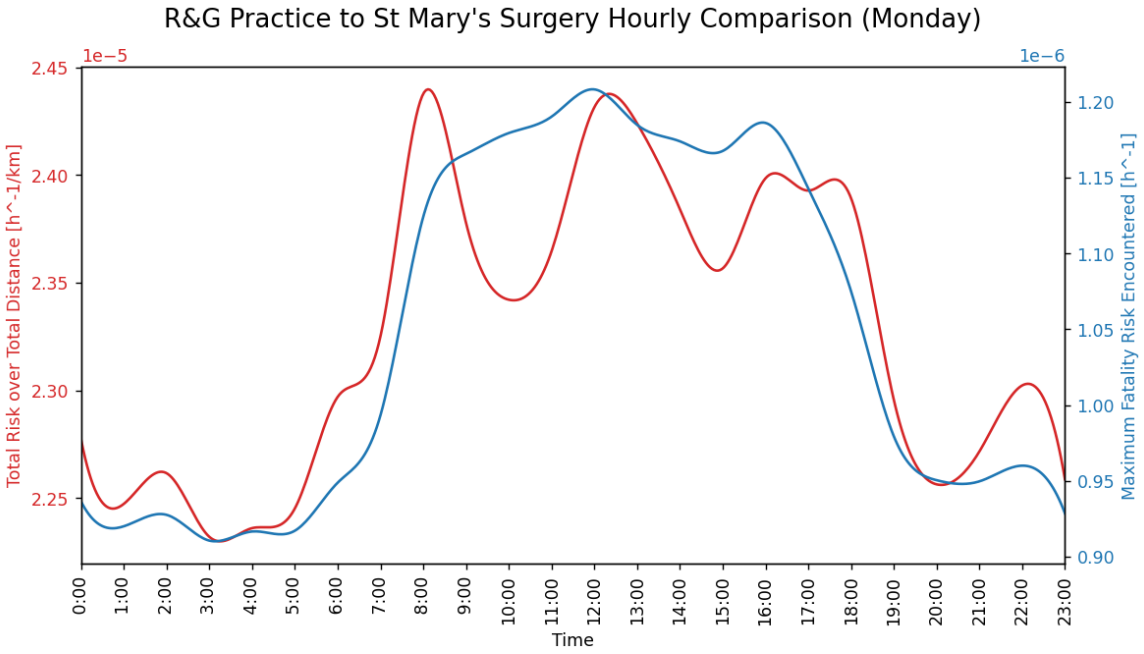

Figure 30: Plot of total risk over total distance as well as maximum fatality risk encountered by a UAS travelling from R&G Practice to St Mary's Surgery during a normal Monday.

However, more interesting was the result when summing all the risk along the path and dividing it by the distance travelled. As seen above, there exist several pockets throughout the day where the total risk per kilometre travelled was significantly lower than expected. This was likely due to a reduction of the population in transit and as such a greater proportion of people are sheltered within origin and destination locations. When taking the entire 24-hour period into account, the ideal timing for performing UAS deliveries in this scenario would be around 10:00 or 15:00 when sticking to surgeries' operating times or 20:00 as a compromise between getting the lowest risk at a slightly inconvenient time while not disturbing the local populace.

5.3 Discussion

It can be seen in both the Southampton City and Hampshire County case study that risk mapping is a potential tool that UAS operators can use to plot safer flightpaths with. However, it should be noted here that the usage of upsampled low resolution data would reduce the accuracy of the results obtained in the previous subsections. The framework laid out by Martin et al. (2015) and implemented in Population24/7 is able to provide high-fidelity spatiotemporal data of the population all the way up to individual buildings or postcodes if sufficient information was available to derive origin/destination containers and time profiles with. As a proof of concept and for the sake of simplicity, the software's default resolution of 200 m by 200 m per cell was used instead.

Additionally, upsampling the data with bilinear interpolation in order to increase the resolution would distort the shape of the population distribution where neighbouring cells would look more continuous even when they are not (a woodland next to a high-density residential area would be better modelled as a discrete jump rather than a linear increase between two data points). Creating more pixels from bilinear interpolation would also result in an incorrect population count as additional population members were added to fill the new containers. However, this would not affect fatality risk calculations as the total population of the raster increases as well. A better but more complex interpolation method such as sum resampling could be implemented instead where values between existing cells are distributed into new ones to maintain the total sum of a raster.

Regarding the results itself, it can be seen that the usage of a different population model does have a significant effect on the generated risk maps. Previous work by Pilko et al. (2022) used NHAPS data and residential area geometries to estimate the temporal and spatial aspects of population movement respectively, resulting in a relatively discretised raster where a large number of cells share the same density with their neighbours. On the other hand, the usage of the 2011 census data and specific time profiles linking origin/destination containers together in this paper has provided a higher fidelity population distribution where variations are noticeable between pixels instead of bigger geometries. The difference between the two approaches could be seen clearly in Figure 12 where large swaths of the raster were dominated by red geometries indicating an overestimation in the old methodology and gradients of blue highlighted the areas which were left out when only using residential zoning to contain population members. As a result, the higher fidelity model produced a more dispersed risk map where there wasn't a high concentration of risk centred in the city but rather a continuous and wide-spread distribution with lower overall risk.

Nonetheless, this result may not be the most realistic as it is difficult to verify the accuracy of the methodology due to a lack of a "ground truth" model. Without an invasion of privacy, establishing a ground truth model of how a population is distributed spatiotemporally would still largely comprise of assumptions and aggregation. This paper was no exception, with data solely taken from censuses and extrapolated between locations using time profiles describing a typical subpopulation's movement. There is a significant source of statistical bias due to the modifiable areal unit problem in which the scale and shape of aggregation units influences the resulting summary values. Namely, the zonal objects used to count population such as census tracts are arbitrary, modifiable, and subject to the whims of whoever is doing the aggregating (Openshaw, 1983). It is therefore likely that the results seen above, which uses official census boundaries, would be different when using other arbitrary boundaries.

Lastly, the veracity of potential paths computed with the Theta* pathfinding algorithm that a UAS can take between delivery locations is also subject to the user's ability in assigning proper inputs. Varying the heuristic (a rough estimate of the distance between each node and the goal) as well as the risk-distance tolerance yields considerably dissimilar results and as such care should be taken when generating flightpaths from these risk maps.

6 Conclusion

The amalgamation of previous works conducted by Pilko et al. (2022) and Martin et al. (2021) has successfully produced a higher fidelity ground risk model based on spatiotemporal population modelling using censuses and administrative data sources. A case study using the city of Southampton yielded similar fatality risk distributions and the investigation of the wider Hampshire County enabled the creation of near-optimum flightpaths between a few candidate surgeries to minimise the risk of fatality during planned UAS trials for sample collection. It was found that drone deliveries between smaller towns in sparsely populated areas such as the New Forest District would yield significantly lower risks and shorter flight times as compared to flights going in and out of larger cities such as Southampton. This is mainly due to lower population densities as well as the FRZ around Southampton Airport requiring all potential flightpaths originating from the city's east to route either between the Winchester-Eastleigh corridor or Southampton Water in order to reach westerly destinations, a complication which does not hinder smaller towns. From these results, further developments in assessing and verifying UAS operational risks should be undertaken to ease the establishment of proper drone regulations and legislations in the future.

6.1 Limitations

There are several limitations when approaching ground risk mapping with this methodology. For one, generating population distributions with higher fidelity leads to an exponential increase in the computational time required. Additionally, the temporal aspect of the model is solely dependent on time profiles provided by authoritative sources. This framework would not be suitable for locations lacking in this data and the accuracy of the results are heavily subjected to the reliability of these characterisations of population movement. Moving on to the calculation of risk itself, a simple wind calculation was performed to determine how it affects the shape of the ground impact probability function. However, it is likely that other weather phenomena would also change the trajectory of a UAS with LoC and as such care should be taken when using the software to predict fatality risks in places with bad weather. Lastly, the results of a risk map are only relevant for a particular UAS model flying at a specific altitude, and at the exact time the map was generated for. It is possible for risk to fluctuate drastically at the same location in a matter of minutes which the timescales used in this paper could not account for.

6.2 Future Work

While the creation of a high-fidelity ground risk mapping software may make it easier to plan and approve UAS missions based on operating risk, there are still many ways in which this approach to quantifying risk could be improved. Perhaps the most important of which is the ability to determine the exact spatiotemporal distribution of the population. Without a proper "ground truth" model, all subsequent results would be purely speculative and full of assumptions. There have been efforts to remedy this situation by using bulked and anonymised mobile network data to extrapolate the required information as seen in Deville et al. (2014), but it can be assumed that consumer concerns in personal privacy would reasonably discourage any mobile carriers from sharing their location thus rendering this method of modelling improbable. As such, more novel solutions in predicting how human geography changes could be investigated. Apart from this, further improvements could be made on the current model's resolution by scaling either the spatial (from 200 to 100 metres or even by postcodes/ individual buildings) or temporal (from hours to minutes or seconds) domains. Optimising the software could also allow faster computation with the possibility of future "on-the-fly" risk calculations.

References

Ahola, T., Virrantaus, K., Krisp, J. M. & Hunter G. J. (2007). A spatio-temporal population model to support risk assessment and damage analysis for decision-making. International Journal of Geographical Information Science, 21(8), 935-953.

Air Accidents Investigation Branch (Feb. 2021). *AAIB investigation to Alauda Airspeeder Mk II, (UAS, registration n/a) 040719*. GOV.UK.

Ajeh, E. A., Modi, F. J. & Omoregie, I. P. (2022). Health risk estimations and geospatial mapping of trace metals in soil samples around automobile mechanic workshops in Benin city, Nigeria. Toxicology Report, 9, 575-587.

Allianz (n.d.). *The landscape - Uses and benefits of UAS.*

Anderson, M. (2015). Censuses: History and Methods. International Encyclopedia of the Social & Behavioral Sciences (Second Edition), 302-307.

Aubrecht, C., Steinnocher, K. & Huber, H. (2014). DynaPop – population distribution dynamics as basis for social impact evaluation in crisis management. ISCRAM 2014 Conference – Proceedings of the 11th International Conference on Information Systems for Crisis Response and Management, 314-318.

Boloorani, A. D., Shorabeh, S. N., Samany, N. N., Mousivand, A., Kazemi, Y., Jaafarzadeh, N., Zahedi, A. & Rabiei, J. (Jun. 2021). Vulnerability mapping and risk analysis of sand and dust storms in Ahvaz, IRAN. Environmental Pollution, 279, 116859.

Breunig, J., Forman, J., Sayed, S., Audenaerd, L., Branch, A. & Hadjimichael, M. (Jul. 2018). Modeling Risk-Based Approach for Small Unmanned Aircraft Systems. The MITRE Corporation, McLean, VA 22102, USA.

Buchholz, K. (Feb. 2019). Commercial Drones are Taking Off. Statista. [Image Edited] https://www.statista.com/chart/17201/commecial-drones-projected-growth/

Bux, R. K., Haider, S. I., Mallah, A., Shah, Z., Solangi, A. R., Moradi, O. & Karimi-Maleh, H. (Jul. 2022). Spatial analysis and human health risk assessment of elements in ground water of District Hyderabad, Pakistan using ArcGIS and multivariate statistical analysis. Environmental Research, 210, 112915.

Calderwood, D. (Feb. 2021). *AAIB report slams CAA and Airspeeder after demo drone crash.* Flyer.

Çalhan, A. & Cicioğlu, M. (Mar. 2022). Drone-assisted smart data gathering for pandemic situations. Computers & Electrical Engineering, 98, 107769.

Ciobanu, E. (2021). *How Often Do Drones Crash or Fly Away?* Droneblog.

Civil Aviation Act (1982) Retrieved November 23, 2021, from https://www.legislation.gov.uk/ukpga/1982/16/contents

Dalamagkidis, K., Valavanis, K. P. & Piegl, L. A. (Oct. 2008). On unmanned aircraft systems issues, challenges and operational restrictions preventing integration into the National Airspace System. Progress in Aerospace Sciences, 44, 503-519.

Daniel, K., Nash, A., Koenig S. & Felner, A. (2010). Theta*: Any-Angle Path Planning on Grids. Journal Of Artificial Intelligence Research, 39, 533-579

Deville, P., Linard, C., Martin, S., Gilbert, M., Stevens, F. R., Gaughan, A. E., Blondel, V. D. & Tatem, A. J. (Nov. 2014). Dynamic population mapping using mobile phone data. Proceedings of the National Academy of Sciences of the United States of America, 111(45), 15888-15893.

Eicher, C. L. & Brewer, C. A. (2001). Dasymetric mapping and areal interpolation: Implementation and evaluation. Cartography and Geographic Information Science, 28(2), 125-138.

Embention (Feb. 2021). *The future of UAVs in logistic industry*.

EUR-Lex (Jun. 2019). *Commission Implementing Regulation (EU) 2019/947 of 24 May 2019 on the rules and procedures for the operation of unmanned aircraft (Text with EEA relevance.)*.

Gershuny, J. & Sullivan, O. (2017). United Kingdom Time Use Survey (TUS), 2014-2015. Centre for Time Use Research, University of Oxford. [Data collection]. UK Data Service. SN: 8128, http://doi.org/10.5255/UKDASN-8128-1.

Ghelichi, Z., Gentili, M. & Mirchandani, P. B. (Nov. 2021). Logistics for a fleet of drones for medical item delivery: A case study for Louisville, KY. Computers & Operations Research, 135, 105443.

Google Maps. (2022). Southampton. Satellite image.

Google My Maps. (2022). Bishop Waltham's Directions. Default image.

Hagerstrand, T. (1970). What about people in regional science? Papers in Regional Science, 24(1), 6-21.

Harris, F. J. (2004). "2.2". Multirate Signal Processing for Communication Systems. Upper Saddle River, NJ: Prentice Hall. pp. 20–21.

Jiang, T., Geller, J., Ni, D. & Collura, J. (Oct. 2016). Unmanned Aircraft System traffic management: Concept of operation and system architecture. International Journal of Transportation Science and Technology, 5(3), 123-135.

JigSpace (Mar. 2020). *Augmented reality product training with Swoop Aero*.

Kersley, A. (Aug. 2021). *The slow collapse of Amazon's drone delivery dream*. Wired UK.

Kesteloo, H. (Jan. 2021). *SWOOP AERO AND SKYPORTS TO OFFER UK-WIDE DRONE DELIVERY SERVICE*. DroneXL.

Klepeis, N. E., Nelson, W. C., Ott, W. R., Robinson, J. P., Tsang, A. M., Switzer, P., Behar, J. V., Hern, S. C. & Engelmann, W. H. (2001). The National Human Activity Pattern Survey (NHAPS): A Resource for Assessing Exposure to Environmental Pollutants. Journal of Exposure Analysis and Environmental Epidemiology, 11, 231-252.

Kraus, J., Kleczatský, A. & Hulínská, S. (2020). Social, technological, and systemic issues of spreading the use of drones. Transportation Research Procedia, 51, 3-10.

Lemardelé, C., Estrada, M., Pagès, L. & Bachofner, M. (May 2021). Potentialities of drones and ground autonomous delivery devices for last-mile logistics. Transportation Research Part E: Logistics and Transportation Review, 149, 102325.

Lynn, K. L. T., Beng, C. L., Guihyun, P., Kin, H. L. & Victor, C. S. Y. (Feb. 2021). Public acceptance of drone applications in a highly urbanized environment. Technology in Society, 64, 101462.

Martin D., Cockings S., Harfoot, A. & Smith, A. D. (2021). Population24/7: an open gridded population dataset for England and Wales. GeoData, University of Southampton.

Martin D., Cockings, S. & Leung, S. (2015). Developing a flexible framework for spatiotemporal population modeling. Annals of the Association of American Geographers, 105(4), 754-772.

Mennis, J. (Mar. 2009). Dasymetric mapping for estimating population in small areas. Geography Compass, 3(2), 727-745.

Modha, A. (Aug. 2021). *ANRA Launches SmartSkies SORA for Its Expanding Portfolio, Closes Funding Round*. ANRA Technologies.

Network Rail (Nov. 2021). *Milestone drone flight for our railway*.

Okabe, A., Boots, B., Sugihara, K. & Chiu, S. N. (2000) Spatial Tessellations: Concepts and Applications of Voronoi Diagrams (Wiley, New York).

OmniSci (2021). *GeoTIFF Definition*.

Openshaw, S. (1983). The modifiable areal unit problem. Norwick: Geo Books.

Oppenheim, A. V., Schafer, R. W. & Buck, J. R. (1999). "4.6.2". Discrete-Time Signal Processing (2nd ed.). Upper Saddle River, NJ.: Prentice Hall. p. 172.

Padró, J., Carabasssa, V., Balagué, J., Brotons, L., Alcañiz, J. M. & Pons, X. (Mar. 2019). Monitoring opencast mine restorations using Unmanned Aerial System (UAS) imagery. Science of The Total Environment, 657, 1602-1614.

Pierce, D. (Dec. 2013). *Delivery drones are coming: Jeff Bezos promises half-hour shipping with Amazon Prime Air*. The Verge.

Pilko, A., Sóbester, A., Scanlan, J. P. & Ferraro, M. (Jan. 2022). Spatiotemporal Ground Risk Mapping for Uncrewed Aerial Systems operations. AIAA SCITECH 2022 Forum.

Pilko, A. & Tait, Z. (2021). Seedpod_ground_risk. GitHub repository. https://github.com/aliaksei135/seedpod_ground_risk

Pop247NRT Project (ES/P010768/1): Data library, sample outputs and batch files for England, 2011 Version 2-0 20/04/21.

Primatesta, S., Rizzo, A. & la Cour-Harbo, A. (May 2019). Ground Risk Map for Unmanned Aircraft in Urban Environments. Journal of Intelligent & Robotic Systems, 97, 489-509.

Pugliese, L. D. P., Guerriero, F. & Macrina, G. (2020). Using drones for parcels delivery process. Procedia Manufacturing, 42, 488-497.

Renner, K., Schneiderbauer, S., Pruß, F., Kofler, C., Martin, D. & Cockings, S. (Mar. 2018). Spatio-temporal population modelling as improved exposure information for risk assessments tested in the Autonomous Province of Bolzano. International Journal of Disaster Risk Reduction, 27, 470-479.

Rey, R. O., Santos de Melo, R. R. & Costa, D. B. (Nov. 2021). Design and implementation of a computerized safety inspection system for construction sites using UAS and digital checklists – Smart Inspecs. Safety Science, 143, 105430.

The Air Navigation Order (2016). Retrieved November 23, 2021, from https://www.legislation.gov.uk/uksi/2016/765/contents/made

Tobler, W. R. (Feb. 1979). Smooth pycnophylactic interpolation for geographical regions. Journal of the American Statistical Association, 74(367), 519-530.

Ueland, S. (Jan. 2021). *8 Commercial Drone Delivery Companies.* PracticalEcommerce.

UK Civil Aviation Authority (2021). *UK EU transition.*

UK Civil Aviation Authority (2020a). *CAP 722: Unmanned Aircraft System Operations in UK Airspace – Guidance*.

UK Civil Aviation Authority (2020b). *Innovation Hub, Beyond Visual Line of Sight in Non-Segregated Airspace: Fundamental Principles & Terminology*.

Wasser, L. A., Jones, M. A., Brym, Z., Riemer, K., Williams, J., Hollister, J. & Smorul, M. (Apr. 2021). Raster 00: Intro to Raster Data in R, National Ecological Observatory Network (NEON).

Wright, D. (Jun. 2014). Drones: Regulatory challenges to an incipient industry. Computer Law & Security Review, 30(3), 226-229.

Wright, J. K. (Jan. 1936). A method of mapping densities of population with Cape Cod as an example. Geographical Review, 26, 103-110.

Zhang, J., Campbell, J. F., Sweeney, D. C. & Hupman, A. C. (Jan. 2021). Energy consumption models for delivery drones: A comparison and assessment. Transportation Research Part D: Transport and Environment, 90, 102668.

Appendix

Appendix 1: Data sources used in Southampton case study (Pop247NRT Project, 2021)

Population sub-groups/ containers	Data source details	Data source URLs (accessed 01/12/2021)	Time profile data
Origins			
Residential locations, including communal	2011 census tables: QS103EW Age by single year (usual residents); LC4411EW - Student accommodation by age; QS421EW - Communal establishment management and type – People	https://www.nomisweb.co.uk/census/2011	Term time/out of term time based on ONS census definitions
Destinations			
Workplaces	2011 census Workplace Population tables: WP1101EW Sex by single year of age; WP605EW Industry; WP601EW Employment Status; WP702EW Distance travelled to work	https://www.nomisweb.co.uk/census/2011	Working patterns by bespoke standard industry classification (SIC) groups, derived from Gershuny and Sullivan (2017)
Primary and Secondary schools	School Census and Independent School Census datasets, pupil numbers, postcode	1) https://www.gov.uk/government/statistics/schools-pupils-and-their-characteristics-january-2011 2) https://webarchive.nationalarchives.gov.uk/20130107054734/http:/www.education.gov.uk/schools/performance/2011/download_data.html 3) https://get-information-schools.service.gov.uk/	Terms and hours estimated clerically from education authority websites. Average attendance
Further Education colleges	Identified from combination of schools census and Higher Education Statistics Agency (HESA) data, based on age profile of students (100% in 16-17 sub-group), enrolled student numbers, postcode	School's census and performance data as above; HESA data as below	Assigned clerically based on planned and funded hours and on proportion of full-time/part-time students
Universities	Higher Education Statistics Agency (HESA) data, enrolled student numbers, postcode	https://www.hesa.ac.uk/	UG/PGT assigned clerically based on University of Southampton Geography average contact time and calendar PGR profile based on office-based workplace profile

Health care facilities	Attendance figures at NHS Trusts, Primary Care Trusts, Treatment Centres, Independent Sector Healthcare Provider sites, distances travelled, postcode	https://digital.nhs.uk/data-and-information/data-tools-and-services/data-services/hospital-episode-statistics	Inpatients allocated clerically by historical bed occupancy data (no longer available); outpatients clerically by estimated appointment times; A&E by mean arrivals over 24 hours
Background			
Road network	Ordnance Survey (OS) OpenMap – Local Road network, Department for Transport (DfT) annual average daily flows (AADF) by area, road, and vehicle type for 19 time periods from National Transport Model	1) https://osdatahub.os.uk/downloads/open 2) http://www.dft.gov.uk/traffic-counts/	Time periods referenced to National Transport Model
Coastline	ONS 2015 Regions, clipped to Mean High Water mark	http://geoportal.statistics.gov.uk/datasets/regions-december-2015-full-clipped-boundaries-in-england	N/A
Inland water	OS OpenMap - Local Surface water	https://osdatahub.os.uk/downloads/open	N/A
Lookup files			
Grid references and lookup files	ONS Postcode Directory November 2012 version; Output Area and Workplace Zone 2011 population-weighted centroids	https://geoportal.statistics.gov.uk/	N/A